

The Sharpin interactome reveals a role for Sharpin in lamellipodium formation via the Arp2/3 complex

Meraj H Khan^{1,2}, Siiri I Salomaa^{1,3}, Guillaume Jacquemet^{1,4}, Umar Butt^{1,2}, Mitro Miihkinen^{1,3}, Takahiro Deguchi^{2,5}, Elena Kremneva⁶, Pekka Lappalainen⁶, Martin J Humphries⁴, Jeroen Pouwels^{1,7}.

¹Turku Centre for Biotechnology, University of Turku, Turku, Finland, ²Turku Doctoral Programme of Molecular Medicine, University of Turku, Turku, Finland, ³Turku Drug Research Doctoral Programme, University of Turku, Turku, Finland, ⁴Wellcome Trust Centre for Cell-Matrix Research, Faculty of Life Sciences, University of Manchester, Manchester, UK., ⁵Laboratory of Biophysics, University of Turku, Turku, Finland. ⁶Institute of Biotechnology, University of Helsinki, Helsinki, Finland.

⁷Corresponding author and lead contact: jerpou@utu.fi

Key words: Sharpin; LUBAC; Arp2/3; linear ubiquitination; interactome

Summary

Sharpin, a multifunctional adaptor protein, regulates several signalling pathways. For example, Sharpin enhances signal-induced NF- κ B signalling as part of the linear ubiquitin assembly complex (LUBAC) and inhibits integrins, the T cell receptor, caspase1 and PTEN. However, despite recent insights into Sharpin and LUBAC function, a systematic approach to identify signalling pathways regulated by Sharpin has not been reported. Here, we present the first ‘Sharpin interactome’, which identifies a large amount of novel potential Sharpin interactors in addition to several known ones. These data suggest that Sharpin and LUBAC might regulate a larger number of biological processes than previously identified, such as endosomal trafficking, RNA processing, metabolism and cytoskeleton regulation. Importantly, using the Sharpin interactome we have identified a novel role for Sharpin in lamellipodium formation. We demonstrate that Sharpin interacts with Arp2/3, a protein complex that catalyses actin filament branching. We identified the Arp2/3-binding site in Sharpin and demonstrate using a specific Arp2/3-binding deficient mutant that the Sharpin-Arp2/3 interaction promotes lamellipodium formation in a LUBAC-independent fashion.

Introduction

Sharpin (SHANK-Associated RH Domain Interactor) is a multifunctional adaptor protein that is amplified (BioPortal.org; (Jung et al., 2010)) and overexpressed (Bii et al., 2015; De Melo and Tang, 2015; He et al., 2010) in many human cancers and promotes cancer cell proliferation, tumour formation and metastasis (Bii et al., 2015; He et al., 2010; Li et al., 2015; Zhang et al., 2014). The most studied function of Sharpin is as part of the linear ubiquitin assembly complex (LUBAC) (Gerlach et al., 2011; Ikeda et al., 2011; Tokunaga et al., 2011), which also includes RBCK1 (RanBP-Type And C3HC4-Type Zinc Finger Containing 1) and the catalytic subunit RNF31 (Ring Finger Protein 31). LUBAC was identified as a regulator of canonical NF- κ B (Nuclear factor-kappaB) signalling (Gerlach et al., 2011; Tokunaga et al., 2009), but it has become evident that LUBAC regulates several other signalling pathways through a growing range of substrates (Chattopadhyay et al., 2016; Dubois et al., 2014; Rodgers et al., 2014; Zak et al., 2011). Consistent with these findings, LUBAC is linked to several diseases, such as autoinflammation, immunodeficiency, amylopectinosis and lymphangiectasia (Boisson et al., 2015; Lewis et al., 2015) and cancer (Yang et al., 2014; Yang et al., 2016).

In addition to its role in linear ubiquitination, Sharpin also binds and inhibits integrins (Pouwels et al., 2013; Rantala et al., 2011), the T cell receptor (Park et al., 2016) and caspase1 (Nastase et al., 2016) in a LUBAC-independent manner. Furthermore, Sharpin functionally interacts with PTEN (Phosphatase And Tensin Homolog) (He et al., 2010), SHANK (SH3 And Multiple Ankyrin Repeat Domains) proteins (Lim et al., 2001) and EYA (Eyes Absent; EYA Transcriptional Coactivator And Phosphatase) transcription factors (Landgraf et al., 2010).

The Arp2/3 (Actin Related Protein 2/3) complex is an actin nucleator that consists of seven subunits (Arp2, Arp3 and ArpC1-5 (Arp2/3 complex subunit 1-5)) and specifically catalyses formation of branched actin filament structures, which play a role in several key cellular functions (Rotty et al., 2013). At the leading edge of migrating cells Arp2/3 creates a dense dendritic meshwork of actin filaments that provides the protrusive force for lamellipodium formation and, thus, cell migration (Rogers et al., 2003; Wu et al., 2012). The Arp2/3 complex depends on nucleation promoting factors (NPFs) such as WASP (Wiskott-Aldrich syndrome protein) and WAVE (WASP family Verprolin-homologous) for full activation, while other proteins inhibit formation of branched actin networks or cause their disassembly (Krause and Gautreau, 2014; Rotty et al., 2013). Importantly, NPFs themselves are subject to strict regulation and can for example be activated through interaction with the small GTPase RAC1 (Rotty et al., 2013).

Despite these discoveries in the linear ubiquitin field and the range of Sharpin interactors, a systematic approach to map proteins and signalling pathways regulated by Sharpin and/or LUBAC has not been reported. Here, we present the first ‘Sharpin interactome’, which identifies many potential Sharpin interactors and suggests that Sharpin, and possibly LUBAC, could regulate a wide range of key biological processes. In addition, we describe a novel direct interaction between Sharpin and the Arp2/3 complex, which is mediated by the Sharpin Ubiquitin like (UBL) domain. Using a specific Arp2/3 binding-deficient Sharpin mutant we describe a novel role for Sharpin in lamellipodium formation that depends on Sharpin interaction with the Arp2/3 complex but is independent of LUBAC function.

Results

Mass spectrometry analyses identify several actin-associated proteins as novel Sharpin interactors

To identify new Sharpin-binding partners and systematically map Sharpin functions, GFP pull-downs from cells expressing GFP-Sharpin or GFP alone were analysed by mass spectrometry (MS). As Sharpin preferentially binds inactive integrins (Rantala et al., 2011), we aimed to identify proteins that associate with Sharpin in an integrin-dependent manner using GFP-Sharpin-expressing cells that were either kept in suspension (integrins mostly inactive; GFP-Sharpin suspension dataset) or plated on fibronectin (integrins mostly active; GFP-Sharpin adherent dataset). Two biological repeats were performed and, in total, 3083 proteins were detected above a set detection threshold (Fig. S1A and Table S1).

To assist in the interrogation and visualisation, proteins were hierarchically clustered using normalised spectral counts as a measure of protein abundance (Fig. S1B). No major differences were observed between the “GFP-Sharpin suspension” and “GFP-Sharpin adherent” datasets (Fig. S1A,B) and, in addition, very few integrin-related proteins were identified (Table S1), which could be due to the fact that integrins are notoriously difficult to co-immunoprecipitate.

To list and score putative Sharpin interactors three thresholds (Low, medium and high confidence; see experimental procedures) were used, reflecting the quality and the specificity of the binding to GFP-Sharpin (Table S1).

Importantly, we identified both other members of the LUBAC complex (RBCK1 and RNF31), as well as many proteins known to associate with LUBAC (Fig. S1C), confirming the validity of the screen. The most established role of Sharpin and LUBAC is regulation of

NF- κ B function. While the NF- κ B transcription factors were not identified, many proteins known to associate with NF- κ B were, further validating the screen (Fig. S1D).

To define the gross composition of proteins recruited to Sharpin (medium threshold) in an unbiased manner, functional annotation clustering based on Gene Ontology (GO; Biological Process_5) was performed using DAVID (Huang da et al., 2009) and displayed as network-based enrichment maps (Merico et al., 2010) (Fig. 1A, Table S2). In total, 261 Biological Processes were over-represented in the GFP-Sharpin datasets. We identified some Biological Processes known to be regulated by Sharpin and LUBAC, such as regulation of cell death (Gerlach et al., 2011; Kumari et al., 2014; Nastase et al., 2016; Rickard et al., 2014), ubiquitin-based processes and cell signalling, the latter of which contains NF- κ B signalling (Fig. 1A, Table S2). In addition, we identified several Biological Processes that have not been associated with Sharpin or LUBAC, such as protein transport, metabolic processes, regulation of the cell cycle and DNA/RNA-based processes, which could suggest that Sharpin and, possibly, LUBAC have a much broader function in cells than described until now. For hypothesis generation and future experimental design, proteins recruited to Sharpin and identified in the above Biological Process categories are short-listed and available as Supporting Information (Table S2). Furthermore, all mass spectrometry proteomics data have been deposited to the ProteomeXchange Consortium via the PRIDE (Vizcaino et al., 2010; Vizcaino et al., 2013) partner repository with the dataset identifier PXD004734 and 10.6019/PXD004734.

The GO analyses also suggest that Sharpin may regulate the cytoskeleton. To identify all cytoskeleton regulators among the proteins recruited to Sharpin, GO analyses using the low threshold list were performed (Table S3), and proteins belonging to the GO term “regulation of cytoskeleton organization” were extracted and hierarchically clustered (Fig. 1B). From this list we selected the Arp2/3 complex for further analysis, as two members of the Arp2/3

complex (ArpC2 and ArpC5), as well as many Arp2/3-associated proteins were identified in the screen (Fig. 1C). Some of these Arp2/3-associated proteins are well-established Arp2/3 regulators, such as GRB2 (Carrier et al., 2000), and cdc42 (Rohatgi et al., 1999).

Sharpin and the Arp2/3 complex interact directly in cells and in vitro

We confirmed the Sharpin-Arp2/3 interaction using several techniques. A proximity ligation (PLA) assay (Soderberg et al., 2006) in HeLa cervical cancer cells showed PLA signals for endogenous Sharpin and Arp2 that were similar to PLA signals for the known interaction pairs α 2-integrin/Sharpin and Arp2/actin (Fig. 2A), indicating interaction between Sharpin and the Arp2/3 complex. The specificity of the PLA was confirmed using antibodies against GFP (Fig. 2A) and irrelevant cytoplasmic proteins (Fig. S2A). In addition, the Arp2-Sharpin PLA signal was significantly reduced in Sharpin silenced cells (Fig. S2B-E). The interaction between endogenous Sharpin and the Arp2/3 complex was verified using co-immunoprecipitation experiments with two different Sharpin antibodies from HEK-293 cell extracts (Fig. 2B; Arp2 was detected as a representative for the whole Arp2/3 complex). In addition, in HEK-293 cells endogenous Arp2/3 was pulled down with overexpressed GFP-Sharpin, but not GFP alone (Fig. 2C). Furthermore, we performed fluorescence resonance energy transfer (FRET) measurements between co-expressed mCherry-Sharpin and Arp3-GFP (Fig. 2D) or GFP-Sharpin and Arp3-TagRFP (Fig. 2E) using fluorescence lifetime imaging microscopy (FLIM). The reduced GFP fluorescence lifetime upon co-expression of Sharpin and Arp3 showed that Sharpin and the Arp2/3 complex interact directly. To further demonstrate the direct interaction we performed an *in vitro* pull-down assay, showing that recombinant GST-Sharpin (Fig. S2F; (Rantala et al., 2011)), but not GST alone, was able to pull-down purified bovine Arp2/3 complex (Fig. 2F). Therefore, we conclude that Sharpin and the Arp2/3 complex interact directly.

To address whether Sharpin regulates Arp2/3 activity we performed an established actin polymerization assay (Fig. 2G), revealing that recombinant GST-Sharpin does not affect actin polymerization induced by Arp2/3, either in the absence or presence of VCA (the WASP verprolin-cofilin-acidic homology domain), which activates Arp2/3 activity (Prehoda et al., 2000). In conclusion, Sharpin and the Arp2/3 complex interact in cells and *in vitro*, but Sharpin does not seem to affect Arp2/3 activity directly *in vitro*.

Interaction between Sharpin and Arp2/3 depends on an intact cytoskeleton and Arp2/3 activity.

To determine whether the actin cytoskeleton is required for the Sharpin-Arp2/3 interaction in cells, we performed PLA and FRET-FLIM experiments, similar as in Fig. 2A and 2E, in the presence or absence of the actin polymerization inhibitor cytochalasin D (CytD). Treatment with CytD strongly reduced PLA between endogenous Sharpin and Arp2, as well as FRET between GFP-Sharpin and Arp3-TagRFP (Fig. S3A,C), showing that the interaction between Sharpin and the Arp2/3 complex depends on an intact cytoskeleton. In addition, 30 minutes treatment with the Arp2/3 inhibitor CK666 (Nolen et al., 2009) also disrupted interaction between Sharpin and Arp2/3 (Fig. S3A,C), but not between Sharpin and α 2-integrin (Fig. S3B), suggesting that Arp2/3 activity is required for the Sharpin-Arp2/3 interaction. Sharpin acts as a negative regulator of integrin activity (Rantala et al., 2011). The disturbed interaction between Arp2/3 and Sharpin after CK666 treatment is not due to differences in integrin activity, however, as these treatments did not affect integrin activity, as shown using total internal reflection fluorescence (TIRF) imaging (Fig. S3D) and fluorescence-activated cell sorting (FACS) analyses (Fig. S3E).

Identification of a specific Arp2/3-binding deficient Sharpin mutant

The Sharpin protein has three conserved functional domains; an N-terminal pleckstrin homology (PH) superfold (Lim et al., 2001; Stieglitz et al., 2012), a central ubiquitin like (UBL) domain that binds most known Sharpin interacting proteins (De Franceschi et al., 2015) and a C-terminal NPL4 zinc finger domain (NZF) that mediates interaction with the T cell receptor (Park et al., 2016) and contributes to LUBAC function (Ikeda et al., 2011). To address which domain mediates interaction with Arp2/3 we used GFP-Sharpin fragments spanning the entire protein (De Franceschi et al., 2015). FRET-FLIM experiments using Arp3-TagRFP and WT or fragment GFP-Sharpin in HeLa cells (Fig. 3A) and pull-down of endogenous Arp2 with WT or fragment GFP-Sharpin from HEK-293 cells (Fig. 3B) showed that the Arp2/3 complex binds to the UBL domain of Sharpin, further confirming the UBL domain as a protein interaction hub.

Using a panel of point mutations of the Sharpin UBL domain we recently showed that the integrin and RNF31 binding domains in the UBL domain partially overlap (De Franceschi et al., 2015). FRET-FLIM experiments between these GFP-Sharpin point mutants and Arp3-TagRFP identified three mutations (V240A/L242A, V267A and L276A) that abolished Arp2/3 binding (Fig. 3C). The other mutants (E260A/L261A, L261A/F263A and I272A) interacted with the Arp2/3 complex, although binding was reduced compared to WT (Fig. 3C). Importantly, the V240A/L242A mutant seems to be specifically unable to bind Arp2/3 as it does not interfere with Sharpin-mediated integrin inhibition and NF- κ B activation (De Franceschi et al., 2015). The V267A and L276A mutations, on the other hand, also abolish the ability of Sharpin to regulate integrins and NF- κ B (De Franceschi et al., 2015). The decreased ability of V240A/L242A GFP-Sharpin to interact with endogenous Arp2 in pull-down assays (Fig. 3D), as compared to WT GFP-Sharpin, confirmed the important role of these residues in binding the Arp2/3 complex. In conclusion, these experiments map the

Arp2/3 interaction site in the Sharpin UBL domain and, importantly, identify a Sharpin mutant (V240A/L242A) that is specifically unable to bind the Arp2/3 complex.

Localization of Sharpin and the Arp2/3 complex in cells

Both Sharpin (Rantala et al., 2011) and the Arp2/3 complex (Rogers et al., 2003; Wu et al., 2012) were reported to localize to lamellipodia. We also observed both proteins in lamellipodia of HeLa cells (Fig. S4A,B) and NCI-H460 lung cancer cells (Fig. S4C). However, the fluorescence intensities suggested that, relative to their cytoplasmic levels, endogenous Arp2 is more enriched in lamellipodia than Sharpin. To quantify this, we measured endogenous Sharpin and Arp2 levels in lamellipodia and the cytoplasm of NCI-H460 cells with line scans, confirming that Arp2 accumulates more in lamellipodia (Fig. S4C). This might suggest that Sharpin is cytoplasmic and that Sharpin localization to lamellipodia is due to cytosolic thickening. To address this, we determined colocalisation of Sharpin and p65 (an NF- κ B subunit that is mostly cytoplasmic in unstimulated cells) and analysed their enrichment in lamellipodia (Fig. S4D). These data show that Sharpin and p65 accumulate to similar levels in lamellipodia and, therefore, Sharpin in lamellipodia is likely cytoplasmic.

If Sharpin localization in lamellipodia is a result of cytoplasmic thickening, Sharpin should not localize to lamellipodia in cells that form flat lamellipodia. Therefore, we analysed accumulation of Sharpin and Arp2 in lamellipodia of U2OS osteosarcoma cells, which showed that, while Arp2 was clearly enriched in such flat lamellipodia, Sharpin accumulation was very limited (Fig. S4E), consistent with Sharpin being a cytoplasmic protein.

Fluorescence recovery after photo bleaching (FRAP) experiments demonstrated that Sharpin in lamellipodia is very dynamic (Fig. S4F, Video S1). However, unlike the Arp2/3 complex, which is incorporated into the actin network at the lamellipodium tip (Lai et al., 2008), GFP-

Sharpin fluorescence recovered evenly throughout the length of the lamellipodium, consistent with simple diffusion of Sharpin in the cytoplasm. Lastly, unlike Arp2, Sharpin was not enriched at actin comets induced by phosphatidylinositol phosphate 5-kinase (PIP5KI) (Fig. S4G; (Rozelle et al., 2000)), consistent with Sharpin being cytoplasmic. All in all, these localization studies show that Sharpin is a cytoplasmic protein and, unlike the Arp2/3 complex, not specifically enriched in lamellipodia.

Sharpin promotes lamellipodium formation

Both Sharpin and Arp2/3 play a role in lamellipodium formation (Rantala et al., 2011; Rogers et al., 2003; Rotty et al., 2013; Wu et al., 2012). Consistent with these studies we observed that Sharpin and Arp3-silenced NCI-H460 lung cancer cells (Fig. S2G,H) formed significantly fewer lamellipodia compared to control silenced cells based on cortactin (Fig. 4A) and filamentous actin (F-actin) staining (Fig. S5A). A similar phenotype was observed in NCI-H460 cells treated for 30 min with CK666 (Fig. 4A). The more pronounced phenotype of the CK666 treated cells compared to Arp3 silencing is most likely due to the strong inhibition of Arp2/3 activity by CK666 (Nolen et al., 2009), while residual Sharpin and Arp3 are present in siRNA transfected cells (Fig. S2G,H). Importantly, silencing of RNF31 (Fig. S2G,H) did not affect lamellipodium formation (Fig. 4A), suggesting that Sharpin promotes lamellipodium formation independent of its role in LUBAC function. Live cell imaging of control silenced NCI-H460 cells, expressing fluorescently tagged Lifeact (Riedl et al., 2008) to visualize F-actin, showed that the lamellipodia are highly dynamic (Video S2). Consistent with the still images (Fig. 4A), Sharpin silenced NCI-H460 cells formed fewer lamellipodia (Video S3). Instead, the surface of Sharpin silenced cells was covered with dynamic filopodia (Video S3), similar to cells with reduced Arp2/3 levels (Video S4; (Beli et al., 2008; Wu et al., 2012)).

To confirm the role of Sharpin in lamellipodium formation and to rule out off-target effects, we created two monoclonal Sharpin knock out NCI-H460 cell lines using CRISPR (Fig. S2I). Consistent with Sharpin facilitating lamellipodium formation, we observed a very robust reduction in lamellipodium formation upon loss of Sharpin (Fig. 4B). Importantly, quantification of lamellipodium formation in control and Sharpin silenced U2OS cells (Fig. S2J) confirmed the role of Sharpin in lamellipodium formation in another cell line and showed that Sharpin also plays a role in the formation of prominent, flat lamellipodia (Fig. 4C).

To investigate lamellipodium dynamics in more detail, we plated control and Sharpin silenced NCI-H460 on line-shaped micropatterns coated with 50 $\mu\text{g/ml}$ fibronectin and 5 $\mu\text{g/ml}$ Alexa488-conjugated fibrinogen and investigated lamellipodium formation after release from CK666 based on cortactin (Fig. 4D) and F-actin staining (Fig. S5B). Consistent with the cells plated on regular coverslips (Fig. 4A), Sharpin silencing strongly reduced the number of cells with lamellipodia on linear micropatterns under unperturbed conditions. Inhibition of Arp2/3 with CK666 abolished formation of lamellipodia in control silenced cells and further reduced the low number lamellipodia in Sharpin silenced cells. As reported previously (Brayford et al., 2016; Haynes et al., 2015), lamellipodia reformed within minutes after CK666 release in control silenced cells. However, such ruffles did not appear in Sharpin silenced cells after CK666 washout (Fig. 4D and S5B), suggesting that Sharpin facilitates formation of lamellipodia rather than stabilizing existing ones.

Sharpin promotes lamellipodium formation through interaction with Arp2/3

To prove that the loss of lamellipodia in Sharpin silenced and knock out cells is specifically due to loss of Sharpin, we performed rescue experiments in NCI-H460 cells (Fig. 5). Expression of WT GFP-Sharpin (insensitive to Sharpin siRNA1 (Rantala et al., 2011))

restored lamellipodium formation (Fig. 5), showing that reduced lamellipodium formation in Sharpin silenced and knock out cells is not due to off-target effects. Importantly, lamellipodium formation was not rescued by the Arp2/3-binding deficient (Fig. 3C,D) GFP-Sharpin (V240A/L242A) (Fig. 5), showing that Sharpin binding to the Arp2/3 complex is essential for Sharpin to promote lamellipodium formation. On the other hand, GFP-Sharpin mutants L261A/F263A and I272A, which are unable to bind RNF31 and support LUBAC function (De Franceschi et al., 2015), rescued lamellipodium formation (Fig. 5A), further supporting the notion that Sharpin supports lamellipodium formation independent of LUBAC.

All in all, these experiments show that Sharpin promotes the lamellipodium formation through interaction with the Arp2/3 complex, independently of LUBAC function.

Sharpin promotes stimulus-induced lamellipodium formation

To address whether Sharpin regulates integrin-mediated lamellipodium formation, we plated WT and Sharpin knock out NCI-H460 cells for 3 h on 5 μ g/ml fibronectin and quantified lamellipodium formation, showing that absence of Sharpin strongly inhibited formation of integrin-dependent lamellipodia in these spreading cells (Fig. S5C). We also observed reduced numbers of integrin-induced lamellipodia upon Sharpin silencing (Fig. S5D), but the effect was smaller, consistent with the modest silencing efficiency in NCI-H460 cells (Fig. S2G,H).

To determine whether Sharpin affects receptor signalling-induced lamellipodium formation we serum starved control or Sharpin silenced U2OS cells overnight and subsequently induced lamellipodium formation through serum stimulation for 120 min (lamellipodium formation was not yet very prominent after 15, 30 and 60 min (data not shown)). In control cells serum starvation abolished lamellipodia, and subsequent release into serum-containing medium

induced a burst of lamellipodia (Fig. 4C). In Sharpin silenced U2OS cells, which make fewer lamellipodia than control cells under unperturbed conditions, we also observed reduced induction of lamellipodium formation after serum release (Fig. 4C), suggesting that Sharpin also regulates receptor signalling-induced lamellipodia.

Finally, to address whether Sharpin also regulates RAC1-driven lamellipodium formation, we expressed constitutively active GFP-RAC1(Q61L) or GFP alone in WT, Sharpin KO1 and Sharpin KO2 NCI-H460 cells. In WT cells we observed the typical shape associated with overexpression of constitutively active RAC1 (Fig. S6A); large flat round cells with very profound lamellipodia all around the edge. GFP-RAC1(Q61L) induced similar shape changes in both Sharpin KO cell lines, as judged by cell area (Fig. S6A), indicating that Sharpin is dispensable for RAC1-driven lamellipodium formation. We confirmed these results using control or Sharpin silenced HeLa cells, in which GFP-RAC1(Q61L) induced similar shape changes (Fig. S6B; also roundness was measured for these cells).

The Sharpin-Arp2/3 interaction promotes cell migration

Arp2/3-dependent lamellipodium formation promotes cell migration, as for example assayed using wound healing assays (Liu et al., 2013; Suraneni et al., 2012). In support of those studies, we also observed decreased wound healing upon silencing of Arp3 in HeLa cells (Fig. S6C). Sharpin silencing, on the other hand, did not affect wound healing under these conditions (Fig. S6C). We have previously observed in several cell lines that Sharpin depletion affects cell migration due to elevated integrin activity (Rantala et al., 2011). Therefore, Sharpin might regulate cell migration through different partners, i.e. inhibition of integrins and stimulation of Arp2/3-dependent lamellipodium formation, which in this wound healing assay seem to cancel each other out.

To address the role of the Sharpin-Arp2/3 interaction in cell migration independent of its role in integrin inactivation, we overexpressed GFP alone, WT GFP-Sharpin or V240A/L242A GFP-Sharpin in Sharpin-deficient (cpdm) Mouse Embryo Fibroblasts (MEFs) (Rantala et al., 2011). Under these conditions, overexpression of WT GFP-Sharpin increased cell migration compared to GFP alone (Fig. 6). Importantly, cpdm MEFs overexpressing V240A/L242A GFP-Sharpin, which is unable to bind the Arp2/3 complex (Fig. 3C,D) and support lamellipodium formation (Fig. 5) but is fully capable of inhibiting integrins (De Franceschi et al., 2015), did not migrate significantly faster than those overexpressing GFP alone (Fig. 6). On the other hand, V240A/L242A GFP-Sharpin overexpressing cpdm MEFs did migrate slower than their WT GFP-Sharpin overexpressing counterparts, suggesting that, under these conditions, Sharpin promotes cell migration through interaction with the Arp2/3 complex, rather than through integrin inhibition.

Altogether, we identify the Arp2/3 complex as a novel Sharpin interactor and show that this interaction plays a role in Arp2/3-dependent lamellipodium formation and could regulate cell migration.

Discussion

Despite rapid developments in the linear ubiquitin field and the clear disease relevance of Sharpin and LUBAC, a comprehensive overview of Sharpin and LUBAC functions is missing. Here, we report the first Sharpin interactome, which potentially links Sharpin and LUBAC to many new pathways, suggesting that Sharpin and LUBAC have a much broader function than reported. In addition, we establish a novel LUBAC-independent function for Sharpin in lamellipodium formation through interaction with the Arp2/3 complex.

Although the vast majority of Sharpin studies focus on LUBAC, several LUBAC-independent functions have been described for Sharpin (Nastase et al., 2016; Park et al.,

2016; Rantala et al., 2011). The LUBAC-independent role for Sharpin in lamellipodium formation through interaction with the Arp2/3 complex described here strengthens the increasingly appreciated notion that Sharpin has important functions outside LUBAC.

Our observation that Sharpin does not accumulate specifically in lamellipodia (Fig. 4) suggests that Sharpin interacts with cytoplasmic Arp2/3, i.e. not associated with the cytoskeleton. This seems counterintuitive with the dependency of the Sharpin-Arp2/3 interaction on an intact cytoskeleton (Fig. S3A,C). However, potentially disruption of the cytoskeleton with CytoD leads to deactivation of Arp2/3, which also disrupts the Arp2/3-Sharpin interaction (Fig. S3A,C). Alternatively, CytoD-mediated disruption of the actin cytoskeleton might affect Sharpin function, for example by affecting post-translational modification of Sharpin or disturbing the interaction between Sharpin and another protein. Consistent with the cytoplasmic Sharpin-Arp2/3 interaction, NPFs were absent from the Sharpin interactome (Table S1) and Sharpin did not affect Arp2/3 activation directly *in vitro* (Fig. 2G). However, we cannot rule out that post-translational modifications of Sharpin or other, yet to be identified proteins could mediate the Sharpin-Arp2/3 interplay in cells. For example, lamellipodium formation could be regulated by a multiprotein interaction, for example a Sharpin-integrin-Arp2/3 complex. Alternatively, the Sharpin-Arp2/3 interaction enhances signalling to the Arp2/3 complex or modulates the Arp2/3-cortactin interaction, consistent with the role for Sharpin in formation of signal-induced lamellipodia (Fig. 4C and S5B,C). Sharpin does not regulate cortactin stability, however, as cortactin levels are largely unaffected in the absence of Sharpin (Fig. S2E,I)

One potential mechanism through which Sharpin could promote lamellipodium formation is stabilisation of the active Arp2/3 conformation, which is consistent with our observations that Arp2/3 levels are modestly reduced upon Sharpin silencing or knockout (Fig. S2E,H,I) and that the Sharpin-Arp2/3 interaction depends on Arp2/3 activity (Fig. S3A,C). Reduced

Arp2/3 levels are unlikely to completely explain the Sharpin phenotype, however, as reducing Arp3 levels with 60% using siRNA in NCI-H460 cells (Fig. S2H) reduced lamellipodium formation by about 50% (Fig. 4A), while lamellipodium formation in Sharpin KO1 NCI-H460 cells, which show modestly reduced Arp2 levels ($24\% \pm 10\%$; Fig S2I), is reduced by about 75% (Fig. 4B).

Lamellipodia induced by constitutively active RAC (GFP-RAC (Q61L)) were not affected by the absence of Sharpin (Fig. S6A,B), which could suggest that Sharpin regulates lamellipodium formation upstream of RAC. However, GFP-RAC (Q61L)-induced lamellipodia in NCI-H460 cells were fully resistant to 6h Arp2/3 inhibition with CK666 (data not shown), suggesting that GFP-RAC (Q61L)-induced lamellipodia are hyperstable. Therefore, while lamellipodia formation is strongly reduced in the absence of Sharpin (NEW figures 4, 5, S5), such lamellipodia could become hyperstable in the presence of GFP-RAC (Q61L), resulting in large flat round cells with profound lamellipodia despite strongly decreased lamellipodium formation rates.

Irrespective of the molecular mechanism, we show that the Sharpin-Arp2/3 interaction is physiologically relevant as it promotes lamellipodium formation (Fig. 5). This might have implications in wound healing and metastasis, although this needs further investigation. The Arp2/3 complex critically regulates several other cellular processes in addition to cell migration (Rotty et al., 2013), but whether Sharpin plays a role in these remains to be established. Interestingly, the Sharpin interactome contains several proteins involved in endocytic trafficking (Table S2), suggesting a role for Sharpin in this Arp2/3-dependent process.

We assigned three different thresholds to objectively score the Sharpin interactors (Table S1). Our 'low threshold' is commonly used in mass spectrometry studies. Importantly, most of the biological functions identified in the Gene Ontology analyses (Fig. 1A) are also represented

in the high threshold list. For example, the proteasome has a very prominent role in the high threshold list, suggesting that Sharpin either binds to or is degraded by the proteasome. Furthermore, in addition to RNF31, two other E3 ubiquitin ligases were identified (RNF114 and STUB1), which could suggest that Sharpin regulates other ubiquitin ligases than LUBAC. Alternatively, Sharpin could be a substrate for these ubiquitin ligases. Interestingly, several Sharpin ubiquitination sites have been identified ((Wagner et al., 2016) and <http://www.phosphosite.org>), although their significance remains unknown.

All in all, we identified several cellular functions that have not been linked to Sharpin and LUBAC (Fig. 1A, Table S2). Therefore, it is tempting to speculate that Sharpin and, potentially, LUBAC have a much broader function than the mostly immunological roles that have been described. Our identification of a novel LUBAC-independent role for Sharpin in regulation of the cytoskeleton shows that the Sharpin interactome can lead to important new insights. We hope that the research community will use this resource to better understand Sharpin and LUBAC function and how these proteins link to cancer and immune-related disease.

Material and Methods

Antibodies

These antibodies were used: rabbit RNF31/HOIP (ab46322, Abcam; 1:1000 western blot (WB)), rabbit GST (91G1, Cell Signaling Technology; 1:1000 WB), rabbit GFP (A11122, Molecular Probes; 1:1000 WB; 1:100 PLA), mouse GFP (ab1218, Abcam; 1:100 PLA), mouse Sharpin (ab69507, Abcam; 1:100 regular IF and PLA; 1 μ g immunoprecipitation), rabbit Sharpin (14626-1-AP, Proteintech; 1:1000 WB; 1 μ g immunoprecipitation), mouse cortactin (p80/85) (05-180, Merck Millipore; 1:300 IF, 1:1000 WB), rabbit Arp2 (ab47654,

Abcam; 1:1000 WB, 1:100 IF), rabbit Arp3 (58182, One World Lab; 1:500 WB), rabbit paxillin (SC-5574, Santa Cruz, 1:100 TIRF), mouse GAPDH (5G4MaB6C5, HyTest; 1:20.000 WB, 1:100 PLA), mouse β -actin (A2228, Sigma; 1:1000 WB, 1:100 PLA), rabbit α 2-integrin (ab1936, Chemicon; 1:100 PLA), rabbit phospho-p44/42 MAPK (Erk1/2) (4370, Cell Signaling Technology; 1:100 PLA), rat 9EG7 (553715, BD Biosciences; 1:100 FACS), mouse P5D2 (Hybridoma bank; 1:20 FACS and TIRF), mouse 12G10 (ab30394, Abcam; 1:100 FACS and TIRF), rabbit p65 (8242, Cell Signaling Technology; 1:100 PLA), rabbit Arpc3 (57646, One World Lab; 1:1000 WB).

These secondary antibodies were Alexa 488- or Alexa 555-conjugated IgGs (Invitrogen; IF), HRP-conjugated IgGs (GE Healthcare; WB), DyLight 680- or 800-conjugated anti-mouse and rabbit IgGs (Thermo Scientific; WB).

Plasmids and siRNAs

Construction of GST-Sharpin and siRNA1-insensitive GFP-Sharpin (Rantala et al., 2011), and Sharpin mutant plasmids (De Franceschi et al., 2015) has been described. Arp3-GFP (Welch et al., 1997) was a gift from Matthew Welch (Addgene Plasmid #8462). Arp3-TagRFP was constructed using primers introducing EcoRI and BamHI sites, followed by cloning into pTagRFP-N (Evrogen). For construction of pmCherry, we replaced GFP in GFP-C1 (Clontech) with mCherry using primers introducing NheI and EcoRI restriction sites. For mCherry-Sharpin, the siRNA1 resistant Sharpin coding sequence was cloned into pmCherry using primers introducing EcoRI and BamHI restriction sites. The mEmerald-Lifeact expression plasmid (mEmerald-Lifeact-7) was from Michael Davidson (Addgene plasmid # 54148). pcDNA3-EGFP-Rac1-Q61L (Subauste et al., 2000) was a gift from the Bokoch lab (Addgene plasmid # 12981). Laura Machesky kindly donated pRK5-Myc-PIP5KIb (Rozelle

et al., 2000). pSpCas9(BB)-2A-GFP (PX458) (Ran et al., 2013) was a gift from Feng Zhang (Addgene plasmid # 48138).

These siRNAs were used: Sharpin (Hs_SHARPIN_1 HP siRNA (Qiagen)), Arp3 (siGENOME Human ACTR3 siRNA (Dharmacon)), RNF31 (siGENOME RNF31 siRNA (Dharmacon)) and control siRNA (AllStars negative control siRNA (Qiagen)).

Synthetic Peptides and Recombinant Proteins

Recombinant GST and GST-Sharpin were produced in *E. coli* Rosetta BL21DE3 and purified according to manufacturer's instructions (BD Biosciences). Arp2/3 complex from bovine brain and GST-tagged human WASP VCA domain were from Cytoskeleton (Cytoskeleton, Inc). Rabbit skeletal muscle actin was purified as described (Pollard and Cooper, 1984).

Cells and Transfections

HeLa cells were grown in DMEM with 10% fetal bovine serum (FBS), 1% L-glutamine, 1% MEM non-essential amino acids, 1% sodium pyruvate, 2% HEPES and 1% penicillin-streptomycin. HEK-293 and U2OS cells were grown in DMEM with 1% penicillin-streptomycin, 10% FBS and 1% L-glutamine. NCI-H460 cells were grown in RPMI1640 with 10% FBS, 1% penicillin-streptomycin, 1% L-glutamine, 1% MEM non-essential amino acids, 1% sodium pyruvate and 1% glucose. The generation and maintenance of cpdm MEF cells has been described (Rantala et al., 2011). All cell lines were regularly tested for contaminations and, except cpdm MEFs, were from American Type Culture Collection (ATCC). Plasmid transfections were done using Lipofectamine 2000 (HeLa and HEK-293 cells) and Lipofectamine 3000 (NCI-H460, U2OS) (Life Technologies). siRNA transfections were done using Hiperfect (Qiagen).

Sharpin knock out cell lines created with CRISPR

Sharpin knockout NCI-H460 cell lines were created using CRISPR genome engineering by excising a defined 488 bp region in the Sharpin gene using two guide RNAs. These guide RNAs (Sigma Aldrich; 5'-TGGCTGTGCACGCCGCGGTG-3', and 5'-TCAGTTTCCTACACCATCCG-3') were designed with MIT CRISPR Designer (<http://crispr.mit.edu/>) and cloned individually in pSpCas9(BB)-2A-GFP (PX458) as described (Ran et al., 2013). Both plasmids were cotransfected into NCI-H460 cells and four days later GFP-positive cells were sorted with FACSaria IIu Cell Sorter (BD Biosciences). Subsequently, we screened for clones that lack the intervening DNA sequence using PCR (forward primer 5'-GTGTCCATTTGTGGGCAAAG and reverse primer 5'-GGCACTGACCATTCTGTCCT) to ensure that the gene is disrupted. Subsequent blotting of two cell lines with the appropriate 488 bp deletion in the Sharpin gene confirmed successful Sharpin knock out. WT control cells went through the same sorting procedure but did not have the deletion and showed normal levels of Sharpin expression.

Mass spectrometry

GFP pulldowns were done using GFP-Trap beads (ChromoTek) according to manufacturer's instructions, with cells kept in suspension or plated on fibronectin (10 µg/ml; Sigma) for 1h before lysis. Protein samples were separated by SDS-PAGE and, following staining with InstantBlue (Expedeon), gel lanes were sliced and subjected to in-gel digestion with trypsin as described (Shevchenko et al., 1996) with modifications (Byron et al., 2015).

Digested samples were analysed by LC-MS/MS using an UltiMate® 3000 Rapid Separation LC (Dionex Corporation) coupled to an Orbitrap Elite (Thermo Fisher Scientific) mass spectrometer. Peptide mixtures were separated using a gradient from 92% A (0.1% FA in water) and 8% B (0.1% FA in acetonitrile) to 33% B, in 44 min at 300 nL/min, using a 75

mm x 250 μm i.d. 1.7 μM BEH C18 analytical column (Waters). Peptides were automatically selected for fragmentation by data-dependent analysis.

Protein identification was done using Proteome Discoverer (1.4) connected to in-house Mascot (v. 2.4) software. Data were searched against the SwissProt database (release 2015_08). Carbamidomethylation of cysteine was set as a fixed modification and oxidation of methionine was allowed as a variable modification. Only tryptic peptides were considered, with up to one missed cleavage permitted. Monoisotopic precursor mass values were used, and only doubly and triply charged precursor ions were considered. Data were validated in Scaffold (version 3.6) using a threshold of identification of at least 50% probability at the peptide level, at least 99% probability at the protein level and assignment of at least two unique, validated peptides. These acceptance criteria resulted in an estimated protein false discovery rate of 0.1% for all datasets. Data were converted using PRIDE Converter (version 2.5.5) (Barsnes et al., 2009) and validated using PRIDE Inspector (version 2.5.2) (Perez-Riverol et al., 2016).

Two biological replicates were performed for each GFP pull-down. Relative protein abundance was calculated using the unweighted spectral count of a given protein normalised to the total number of spectra observed in the entire sample and to the molecular weight of that protein (normalised spectral count). To list and score the putative Sharpin interactors, three thresholds were used, reflecting the quality and the specificity of the binding to GFP-Sharpin. Low confidence was assigned to 690 proteins detected with at least 4 spectra and that were enriched two-fold in the GFP-Sharpin datasets (suspension or adherent) over control. To provide lists of putative Sharpin binders that are likely to contain fewer false positives, two other thresholds were used. A medium confidence was assigned to 297 proteins detected with at least 5 spectra and enriched four-fold in the GFP-Sharpin datasets (suspension or adherent) over control, while a high confidence was assigned to 48 proteins

detected with at least 10 spectra and enriched four-fold in both GFP-Sharpin datasets.

Gene Ontology analyses were performed using DAVID (version 6.8) (Huang da et al., 2009) and the Gene Ontology map created using the Cytoscape plugin “Enrichment Map” (Merico et al., 2010). Proteins were hierarchically clustered on the basis of uncentred Pearson correlation using Cluster 3.0 (CCLustering Library, version 1.50) (de Hoon et al., 2004) and visualized using JavaTreeView (version 1.1.6r2) (Saldanha, 2004). PPI network analyses were performed using Cytoscape (version 3.4.0) (Smoot et al., 2011). Proteins were mapped onto a merged human interactome consisting of PPIs reported in the Protein Interaction Network Analysis platform Homo sapiens network (Wu et al., 2009) integrated within Cytoscape using PINA4MS (version 2.0.1).

Accession numbers.

The mass spectrometry proteomics data have been deposited to the ProteomeXchange Consortium via the PRIDE partner repository with the dataset identifier PXD004734 and 10.6019/PXD004734.

Immunoblottings, Immunoprecipitations and Pull-Downs

All immunoblottings, immunoprecipitations and GFP-bead (ChromoTek) pull-downs were described previously (Pouwels et al., 2013).

For GST pull-down experiments Glutathione Sepharose 4B beads (GE Healthcare) were washed twice with binding buffer (20 mM Tris pH 7.5, 50 mM NaCl, 0.5 mM EDTA and 2 mM MgCl₂) and subsequently incubated with 10 µg GST or GST-Sharpin in binding buffer (1h rotation at 4 °C). After washing, beads were incubated with binding buffer with 2 µM purified Arp2/3 complex and 0.1 mM ATP (1.5 h rotation at 4 °C). Subsequently, beads were washed and suspended into loading buffer. Samples were analysed using immunoblotting.

Immunofluorescence

NCI-H460 or HeLa cells were fixed with 4% paraformaldehyde and stained. Immunofluorescent images in Fig. S4 (except Fig. S4C,D) were obtained with a 3i Marianas Spinning disk confocal microscope, equipped with Yokogawa CSU-W1 scanner (Intelligent Imaging Innovations), ORCA-Flash4.0 v2 sCMOS Camera (Hamamatsu Photonics), and Plan-Apochromat 63x/1.4NA oil objective. Images in Fig. S4G were processed using the super-resolution radial fluctuations (SRRF) ImageJ plugin (Gustafsson et al., 2016). Images in Figures 4, 5 S4C,D and S5 were obtained using a Zeiss AxioVert 200M inverted wide field microscope equipped with Plan-NEOFLUAR 63x/1.25NA oil objective (Zeiss) and Orca-ER camera (Hamamatsu Photonics). All image processing was done using Fiji image analysis software (Schindelin et al., 2012).

Total Internal Reflection Fluorescence Microscopy (TIRF)

HeLa cells, freshly adherent to 3cm glass bottom dishes (MatTek Corporation) coated with 5ug/ml fibronectin, were stained for Active (12G10) or Total (P5D2) integrins, along with Paxillin, F-Actin (Atto Phalloidin) and DAPI. Samples were imaged using a Carl Zeiss Laser-TIRF 3 Imaging System equipped with 63x/1.46NA oil objective (alpha Plan-Apochromat, DIC) and Hamamatsu ImageEM C9100-13 emccd camera (Hamamatsu Photonics). All image analysis was done using Fiji.

Fluorescence Recovery After Photobleaching

GFP-Sharpin expressing NCI-H460 cells on glass-bottom dishes (MatTek Corporation), in Ham's F12 Nutrient Mixture with 10 % FBS and 1% HEPES, were subjected to FRAP imaging with 1s intervals using the 3i Marianas Spinning disk confocal microscope, equipped

as described above. After imaging for approximately 10 seconds, cellular areas were bleached, followed by imaging for 90-120 seconds. FRAP data were analysed using the SlideBook 6 (Intelligent Imaging Innovations) FRAP analysis module. Movies and still images were prepared using Fiji.

Live Cell imaging

NCI-H460 cells expressing mEmerald-Lifeact, plated for 4h in Ham's F12 Nutrient Mixture with 10% FBS and 1% HEPES on glass-bottom dishes (MatTek Corporation) coated with 5 µg/ml fibronectin, were imaged at 37 °C at 5 frames/min for 5-10 min with a Carl Zeiss Laser-TIRF 3 Imaging System equipped as described above. Movies were prepared using Fiji.

For live cell imaging of GFP alone, or WT or V240A/L242A GFP-Sharpin overexpressing cpdm MEFs, cells were plated sparsely in regular medium with 5 % HEPES onto µ-Slide 8 wells (Ibidi) coated with 5 µg/ml fibronectin. Six hours after plating cells were imaged every 10 min with phase-contrast for at least 8h, with GFP images taken every 10 frames. Imaging was done using a 3i Marianas Spinning disk confocal microscope, equipped as described above, except that a 10x objective was used.

For the wound healing assays equal amounts of HeLa cells were plated on an IncuCyte ImageLock™ 96-well plate (Essen BioScience). The next day a wound was made in the confluent monolayer using an Essen BioScience WoundMaker™ and wound closure was imaged every two hours using an IncuCyte Zoom™ System (Essen BioScience) with 10x objective.

Pyrene-actin polymerization assay

For the pyrene-actin mixture, 5% of pyrene-labelled actin was mixed with non-labelled G-actin in G-buffer (5 mM Tris-HCl pH 7.5 with 0.2 mM DTT, 0.2 mM CaCl₂ and 0.2 mM ATP) to a final concentration of 20 μM. 11 μM of GST-Sharpin was mixed with 40 nM Arp2/3 and 30 nM VCA (or equal volume of VCA-buffer) in 50mM Tris-HCl pH 7.5 with 150 mM NaCl, 3 mM DTT and 10% Glycerol in the presence of 1x initiation mix (1 mM EGTA, 5 mM MgCl₂, 0.25 mM ATP and NaCl to the total 100 mM in the final sample). Polymerization of actin filaments was monitored at 22 °C with excitation at 365 nm (Ex. Slit = 10 nm) and emission at 407 nm (Em. Slit = 20 nm) after addition of 4 μM pyrene-actin. Measurements were carried out on an Agilent Cary Eclipse Fluorescence Spectrophotometer with BioMelt Bundle System (Agilent Technologies). Origin 7.5 software (OriginLab Corp.) was used for data analyses.

FACS

HeLa cells, treated for 30 min with DMSO, 10 μM Cytochalasin D (Sigma-Aldrich) or 100 μM CK666 (Sigma-Aldrich), were detached and fixed with 4% paraformaldehyde. Cells were stained for active β1-integrin (12G10) or total β1-integrin (P5D2). Samples were analysed using FACSCalibur with CellQuest software (BD Biosciences) and non-commercial Flowing Software ver. 2.5 (Mr. Perttu Terho; Turku Centre for Biotechnology, Finland; www.flowingsoftware.com). The Integrin Activation Index was calculated by dividing background corrected active cell-surface integrin levels by total cell-surface integrin levels.

Proximity Ligation Assays

PLA assays were carried out according to a previously described protocol (Soderberg et al., 2006). Images were taken with a Carl Zeiss LSM780 laser scanning confocal microscope equipped with 63x/1.2 W Corr Apochromat objective (Zeiss). PLA signals per cell were calculated by dividing the amount of PLA signal dots in one field of view, determined using Cell Profiler software (Carpenter et al., 2006), by the amount of cells, as determined by counting nuclei.

FRET measurements by FLIM

HeLa cells were transfected with donor alone (GFP-Sharpin constructs (WT, fragments, or point mutants) or Arp3-GFP) in control samples, or with donor together with the acceptor (Arp3-TagRFP or mCherry-Sharpin). As an additional control, cells were transfected with Arp3-GFP and mCherry alone. After 24h cells were fixed and mounted with Mowiol 4–88 (Sigma–Aldrich). GFP fluorescence lifetime was measured using a fluorescence lifetime imaging attachment (Lambert Instruments) on a Zeiss AXIO Observer D1 inverted microscope (Zeiss). For sample excitation sinusoidally modulated 3W, 497 nm LED at 40 MHz under epi-illumination was used. Cells were imaged using the 63×, NA 1.4 oil objective (excitation: BP470/40, beam splitter: FT495, emission: BP525/50). The phase and modulation were determined using the manufacturer's software from images acquired at 12 phase settings. Fluorescein at 0.01 mM, pH 9 was used as a lifetime reference standard. The apparent FRET efficiency was calculated using the measured lifetimes of each donor-acceptor pair (τ_{DA}) and the average lifetime of the donor only (τ_D) samples, according to Equation 1.

$$\text{Equation 1: FRET Efficiency} = \left(1 - \left(\frac{\tau_{DA}}{\tau_D} \right) \right) * 100\%$$

Micropatterns

Linear micropatterns with a width of 9 μm were produced on glass coverslips as described (Azioune et al., 2009) and coated with 50 $\mu\text{g/ml}$ fibronectin and 5 $\mu\text{g/ml}$ fibrinogen, Alexa Fluor 488 Conjugate (Thermo Scientific). NCI-H460 cells were seeded in antibiotic-free medium for 7 h, followed by fixing and staining as described above. Cells were observed using a Zeiss AxioVert 200M inverted wide field microscope equipped with Plan-NEOFLUAR 100x/1.25NA oil objective (Zeiss) and Hamamatsu Orca-ER camera (Hamamatsu Photonics). All image processing was done using Fiji.

Statistical Analysis

All statistical analyses were performed using GraphPad Prism version 5.03 for Windows (GraphPad Software). The Student's t-test was used for normally distributed data (Shapiro-Wilk normality test $\alpha=0.05$). For all other data the Mann-Whitney test was used. A $p < 0.05$ was considered significant.

Acknowledgements

We thank K. Ikkala, M. Skaldin, P. Laasola and A. Augenlicht for technical assistance and the Cell Imaging Core at Turku Centre for Biotechnology for assistance with microscopy and flow cytometry. We thank J.D. Humphries, A. Byron, S. Warwood and D. Knight for help with the acquisition and analysis of the mass-spectrometry data. Matthew Welch (UC Berkeley), Laura Machesky (CRUK Beatson Institute), the Bokoch lab (The Scripps Research Institute), Feng Zhang (Broad Institute) and Michael Davidson (Florida State University) are acknowledged for plasmids.

Competing Interests

The authors declare no competing financial interests.

Author contributions

Conceptualization: JP, MK, SS. Methodology: MK, SS, GJ, UB, MM, EK, JP. Analysis: MK, SS, GJ, UB, EK, JP. Investigation: MK, SS, GJ, UB, TD, EK, JP. Writing: MK, SS, GJ, JP. Supervision: PL, MH, JP.

Funding

This work was supported by the University of Turku Graduate School, Doctoral Programmes of Molecular Medicine (MK and TD) and Drug Research (SS and MM), Sigrid Juselius Foundation (PL), Wellcome Trust (grant 092015; MH), Cancer Research UK (grant C13329/A21671; MH) and the Academy of Finland (JP).

Data Availability

The mass spectrometry proteomics data have been deposited to the ProteomeXchange Consortium via the PRIDE partner repository with the dataset identifier PXD004734 and 10.6019/PXD004734.

References

Azioune, A., Storch, M., Bornens, M., They, M. and Piel, M. (2009). Simple and rapid process for single cell micro-patterning. *Lab. Chip* 9, 1640-1642.

Barsnes, H., Vizcaino, J. A., Eidhammer, I. and Martens, L. (2009). PRIDE converter: Making proteomics data-sharing easy. *Nat. Biotechnol.* 27, 598-599.

Beli, P., Mascheroni, D., Xu, D. and Innocenti, M. (2008). WAVE and Arp2/3 jointly inhibit filopodium formation by entering into a complex with mDia2. *Nat. Cell Biol.* 10, 849-857.

Bii, V. M., Rae, D. T. and Trobridge, G. D. (2015). A novel gammaretroviral shuttle vector insertional mutagenesis screen identifies SHARPIN as a breast cancer metastasis gene and prognostic biomarker. *Oncotarget* 6, 39507-39520.

Boisson, B., Laplantine, E., Dobbs, K., Cobat, A., Tarantino, N., Hazen, M., Lidov, H. G., Hopkins, G., Du, L., Belkadi, A. et al. (2015). Human HOIP and LUBAC deficiency underlies autoinflammation, immunodeficiency, amylopectinosis, and lymphangiectasia. *J. Exp. Med.* 212, 939-951.

Brayford, S., Bryce, N. S., Schevzov, G., Haynes, E. M., Bear, J. E., Hardeman, E. C. and Gunning, P. W. (2016). Tropomyosin promotes lamellipodial persistence by collaborating with Arp2/3 at the leading edge. *Curr. Biol.* 26, 1312-1318.

Byron, A., Askari, J. A., Humphries, J. D., Jacquemet, G., Koper, E. J., Warwood, S., Choi, C. K., Stroud, M. J., Chen, C. S., Knight, D. et al. (2015). A proteomic approach reveals

integrin activation state-dependent control of microtubule cortical targeting. *Nat. Commun.* 6, 6135.

Carrier, M. F., Nioche, P., Broutin-L'Hermite, I., Boujemaa, R., Le Clainche, C., Egile, C., Garbay, C., Ducruix, A., Sansonetti, P. and Pantaloni, D. (2000). GRB2 links signaling to actin assembly by enhancing interaction of neural wiskott-aldrich syndrome protein (N-WASp) with actin-related protein (ARP2/3) complex. *J. Biol. Chem.* 275, 21946-21952.

Carpenter, A. E., Jones, T. R., Lamprecht, M. R., Clarke, C., Kang, I. H., Friman, O., Guertin, D. A., Chang, J. H., Lindquist, R. A., Moffat, J. et al. (2006). CellProfiler: Image analysis software for identifying and quantifying cell phenotypes. *Genome Biol.* 7, R100.

Chattopadhyay, S., Kuzmanovic, T., Zhang, Y., Wetzel, J. L. and Sen, G. C. (2016). Ubiquitination of the transcription factor IRF-3 activates RIPA, the apoptotic pathway that protects mice from viral pathogenesis. *Immunity* 44, 1151-1161.

De Franceschi, N., Peuhu, E., Parsons, M., Rissanen, S., Vattulainen, I., Salmi, M., Ivaska, J. and Pouwels, J. (2015). Mutually exclusive roles of SHARPIN in integrin inactivation and NF- κ B signaling. *PloS one* 10(11), e0143423.

de Hoon, M. J., Imoto, S., Nolan, J. and Miyano, S. (2004). Open source clustering software. *Bioinformatics* 20, 1453-1454.

De Melo, J. and Tang, D. (2015). Elevation of SIPL1 (SHARPIN) increases breast cancer risk. *PLoS One* 10, e0127546.

Dubois, S. M., Alexia, C., Wu, Y., Leclair, H. M., Leveau, C., Schol, E., Fest, T., Tarte, K., Chen, Z. J., Gavard, J. et al. (2014). A catalytic-independent role for the LUBAC in NF-

kappaB activation upon antigen receptor engagement and in lymphoma cells. *Blood* *123*, 2199-2203.

Gerlach, B., Cordier, S. M., Schmukle, A. C., Emmerich, C. H., Rieser, E., Haas, T. L., Webb, A. I., Rickard, J. A., Anderton, H., Wong, W. W. et al. (2011). Linear ubiquitination prevents inflammation and regulates immune signalling. *Nature* *471*, 591-596.

Gustafsson, N., Culley, S., Ashdown, G., Owen, D. M., Pereira, P. M. and Henriques, R. (2016). Fast live-cell conventional fluorophore nanoscopy with ImageJ through super-resolution radial fluctuations. *Nat. Commun.* *7*, 12471.

Haynes, E. M., Asokan, S. B., King, S. J., Johnson, H. E., Haugh, J. M. and Bear, J. E. (2015). GMFbeta controls branched actin content and lamellipodial retraction in fibroblasts. *J. Cell Biol.* *209*, 803-812.

He, L., Ingram, A., Rybak, A. P. and Tang, D. (2010). Shank-interacting protein-like 1 promotes tumorigenesis via PTEN inhibition in human tumor cells. *J. Clin. Invest.* *120*, 2094-2108.

Huang da, W., Sherman, B. T. and Lempicki, R. A. (2009). Systematic and integrative analysis of large gene lists using DAVID bioinformatics resources. *Nat. Protoc.* *4*, 44-57.

Ikeda, F., Deribe, Y. L., Skanland, S. S., Stieglitz, B., Grabbe, C., Franz-Wachtel, M., van Wijk, S. J., Goswami, P., Nagy, V., Terzic, J. et al. (2011). SHARPIN forms a linear ubiquitin ligase complex regulating NF-kappaB activity and apoptosis. *Nature* *471*, 637-641.

Jung, J., Kim, J. M., Park, B., Cheon, Y., Lee, B., Choo, S. H., Koh, S. S. and Lee, S. (2010). Newly identified tumor-associated role of human sharpin. *Mol. Cell. Biochem.* *340*, 161-167.

Krause, M. and Gautreau, A. (2014). Steering cell migration: Lamellipodium dynamics and the regulation of directional persistence. *Nat. Rev. Mol. Cell Biol.* *15*, 577-590.

Kumari, S., Redouane, Y., Lopez-Mosqueda, J., Shiraishi, R., Romanowska, M., Lutzmayer, S., Kuiper, J., Martinez, C., Dikic, I., Pasparakis, M. et al. (2014). Sharpin prevents skin inflammation by inhibiting TNFR1-induced keratinocyte apoptosis. *Elife* *3*, 10.7554/eLife.03422.

Lai, F. P., Szczodrak, M., Block, J., Faix, J., Breitsprecher, D., Mannherz, H. G., Stradal, T. E., Dunn, G. A., Small, J. V. and Rottner, K. (2008). Arp2/3 complex interactions and actin network turnover in lamellipodia. *EMBO J.* *27*, 982-992.

Landgraf, K., Bollig, F., Trowe, M. O., Besenbeck, B., Ebert, C., Kruspe, D., Kispert, A., Hanel, F. and Englert, C. (2010). Sipl1 and Rbck1 are novel Eya1-binding proteins with a role in craniofacial development. *Mol. Cell. Biol.* *30*, 5764-5775.

Lewis, M. J., Vyse, S., Shields, A. M., Boeltz, S., Gordon, P. A., Spector, T. D., Lehner, P. J., Walczak, H. and Vyse, T. J. (2015). UBE2L3 polymorphism amplifies NF-kappaB activation and promotes plasma cell development, linking linear ubiquitination to multiple autoimmune diseases. *Am. J. Hum. Genet.* *96*, 221-234.

Li, J., Lai, Y., Cao, Y., Du, T., Zeng, L., Wang, G., Chen, X., Chen, J., Yu, Y., Zhang, S. et al. (2015). SHARPIN overexpression induces tumorigenesis in human prostate cancer LNCaP, DU145 and PC-3 cells via NF-kappaB/ERK/Akt signaling pathway. *Med. Oncol.* *32*, 444-014-0444-3. Epub 2015 Jan 1.

Lim, S., Sala, C., Yoon, J., Park, S., Kuroda, S., Sheng, M. and Kim, E. (2001). Sharpin, a novel postsynaptic density protein that directly interacts with the shank family of proteins. *Mol. Cell. Neurosci.* *17*, 385-397.

Liu, Z., Yang, X., Chen, C., Liu, B., Ren, B., Wang, L., Zhao, K., Yu, S. and Ming, H. (2013). Expression of the Arp2/3 complex in human gliomas and its role in the migration and invasion of glioma cells. *Oncol. Rep.* *30*, 2127-2136.

Merico, D., Isserlin, R., Stueker, O., Emili, A. and Bader, G. D. (2010). Enrichment map: A network-based method for gene-set enrichment visualization and interpretation. *PLoS One* *5*, e13984.

Nastase, M. V., Zeng-Brouwers, J., Frey, H., Hsieh, L. T., Poluzzi, C., Beckmann, J., Schroeder, N., Pfeilschifter, J., Lopez-Mosqueda, J., Mersmann, J. et al. (2016). An essential role for SHARPIN in the regulation of caspase 1 activity in sepsis. *Am. J. Pathol.* *186*, 1206-1220.

Nolen, B. J., Tomasevic, N., Russell, A., Pierce, D. W., Jia, Z., McCormick, C. D., Hartman, J., Sakowicz, R. and Pollard, T. D. (2009). Characterization of two classes of small molecule inhibitors of Arp2/3 complex. *Nature* *460*, 1031-1034.

Park, Y., Jin, H. S., Lopez, J., Lee, J., Liao, L., Elly, C. and Liu, Y. C. (2016). SHARPIN controls regulatory T cells by negatively modulating the T cell antigen receptor complex. *Nat. Immunol.* *17*, 286-296.

Perez-Riverol, Y., Xu, Q. W., Wang, R., Uszkoreit, J., Griss, J., Sanchez, A., Reisinger, F., Csordas, A., Ternent, T., Del-Toro, N. et al. (2016). PRIDE inspector toolsuite: Moving

toward a universal visualization tool for proteomics data standard formats and quality assessment of ProteomeXchange datasets. *Mol. Cell. Proteomics* 15, 305-317.

Pollard, T. D. and Cooper, J. A. (1984). Quantitative analysis of the effect of acanthamoeba profilin on actin filament nucleation and elongation. *Biochemistry* 23, 6631-6641.

Pouwels, J., De Franceschi, N., Rantakari, P., Auvinen, K., Karikoski, M., Mattila, E., Potter, C., Sundberg, J. P., Hogg, N., Gahmberg, C. G. et al. (2013). SHARPIN regulates uropod detachment in migrating lymphocytes. *Cell. Rep.* 5, 619-628.

Prehoda, K. E., Scott, J. A., Mullins, R. D. and Lim, W. A. (2000). Integration of multiple signals through cooperative regulation of the N-WASP-Arp2/3 complex. *Science* 290, 801-806.

Ran, F. A., Hsu, P. D., Wright, J., Agarwala, V., Scott, D. A. and Zhang, F. (2013). Genome engineering using the CRISPR-Cas9 system. *Nat. Protoc.* 8, 2281-2308.

Rantala, J. K., Pouwels, J., Pellinen, T., Veltel, S., Laasola, P., Mattila, E., Potter, C. S., Duffy, T., Sundberg, J. P., Kallioniemi, O. et al. (2011). SHARPIN is an endogenous inhibitor of beta1-integrin activation. *Nat. Cell Biol.* 13, 1315-1324.

Rickard, J. A., Anderton, H., Etemadi, N., Nachbur, U., Darding, M., Peltzer, N., Lalaoui, N., Lawlor, K. E., Vanyai, H., Hall, C. et al. (2014). TNFR1-dependent cell death drives inflammation in sharpin-deficient mice. *Elife* 3, 10.7554/eLife.03464.

Riedl, J., Crevenna, A. H., Kessenbrock, K., Yu, J. H., Neukirchen, D., Bista, M., Bradke, F., Jenne, D., Holak, T. A., Werb, Z. et al. (2008). Lifeact: A versatile marker to visualize F-actin. *Nat. Methods* 5, 605-607.

Rodgers, M. A., Bowman, J. W., Fujita, H., Orazio, N., Shi, M., Liang, Q., Amatya, R., Kelly, T. J., Iwai, K., Ting, J. et al. (2014). The linear ubiquitin assembly complex (LUBAC) is essential for NLRP3 inflammasome activation. *J. Exp. Med.* *211*, 1333-1347.

Rogers, S. L., Wiedemann, U., Stuurman, N. and Vale, R. D. (2003). Molecular requirements for actin-based lamella formation in drosophila S2 cells. *J. Cell Biol.* *162*, 1079-1088.

Rohatgi, R., Ma, L., Miki, H., Lopez, M., Kirchhausen, T., Takenawa, T. and Kirschner, M. W. (1999). The interaction between N-WASP and the Arp2/3 complex links Cdc42-dependent signals to actin assembly. *Cell* *97*, 221-231.

Rotty, J. D., Wu, C. and Bear, J. E. (2013). New insights into the regulation and cellular functions of the ARP2/3 complex. *Nat. Rev. Mol. Cell Biol.* *14*, 7-12.

Rozelle, A. L., Machesky, L. M., Yamamoto, M., Driessens, M. H., Insall, R. H., Roth, M. G., Luby-Phelps, K., Marriott, G., Hall, A. and Yin, H. L. (2000). Phosphatidylinositol 4,5-bisphosphate induces actin-based movement of raft-enriched vesicles through WASP-Arp2/3. *Curr. Biol.* *10*, 311-320.

Saldanha, A. J. (2004). Java treeview--extensible visualization of microarray data. *Bioinformatics* *20*, 3246-3248.

Schindelin, J., Arganda-Carreras, I., Frise, E., Kaynig, V., Longair, M., Pietzsch, T., Preibisch, S., Rueden, C., Saalfeld, S., Schmid, B. et al. (2012). Fiji: An open-source platform for biological-image analysis. *Nat. Methods* *9*, 676-682.

Shevchenko, A., Wilm, M., Vorm, O., Jensen, O. N., Podtelejnikov, A. V., Neubauer, G., Shevchenko, A., Mortensen, P. and Mann, M. (1996). A strategy for identifying gel-separated proteins in sequence databases by MS alone. *Biochem. Soc. Trans.* *24*, 893-896.

Smoot, M. E., Ono, K., Ruscheinski, J., Wang, P. L. and Ideker, T. (2011). Cytoscape 2.8: New features for data integration and network visualization. *Bioinformatics* 27, 431-432.

Soderberg, O., Gullberg, M., Jarvius, M., Ridderstrale, K., Leuchowius, K. J., Jarvius, J., Wester, K., Hydbring, P., Bahram, F., Larsson, L. G. et al. (2006). Direct observation of individual endogenous protein complexes in situ by proximity ligation. *Nat. Methods* 3, 995-1000.

Stieglitz, B., Haire, L. F., Dikic, I. and Rittinger, K. (2012). Structural analysis of SHARPIN, a subunit of a large multi-protein E3 ubiquitin ligase, reveals a novel dimerization function for the pleckstrin homology superfold. *J. Biol. Chem.* 287, 20823-20829.

Subauste, M. C., Von Herrath, M., Benard, V., Chamberlain, C. E., Chuang, T. H., Chu, K., Bokoch, G. M. and Hahn, K. M. (2000). Rho family proteins modulate rapid apoptosis induced by cytotoxic T lymphocytes and fas. *J. Biol. Chem.* 275, 9725-9733.

Suraneni, P., Rubinstein, B., Unruh, J. R., Durnin, M., Hanein, D. and Li, R. (2012). The Arp2/3 complex is required for lamellipodia extension and directional fibroblast cell migration. *J. Cell Biol.* 197, 239-251.

Tokunaga, F., Nakagawa, T., Nakahara, M., Saeki, Y., Taniguchi, M., Sakata, S., Tanaka, K., Nakano, H. and Iwai, K. (2011). SHARPIN is a component of the NF-kappaB-activating linear ubiquitin chain assembly complex. *Nature* 471, 633-636.

Tokunaga, F., Sakata, S., Saeki, Y., Satomi, Y., Kirisako, T., Kamei, K., Nakagawa, T., Kato, M., Murata, S., Yamaoka, S. et al. (2009). Involvement of linear polyubiquitylation of NEMO in NF-kappaB activation. *Nat. Cell Biol.* 11, 123-132.

Vizcaino, J. A., Cote, R., Reisinger, F., Barsnes, H., Foster, J. M., Rameseder, J., Hermjakob, H. and Martens, L. (2010). The proteomics identifications database: 2010 update. *Nucleic Acids Res.* *38*, D736-42.

Vizcaino, J. A., Cote, R. G., Csordas, A., Dianes, J. A., Fabregat, A., Foster, J. M., Griss, J., Alpi, E., Birim, M., Contell, J. et al. (2013). The PRoteomics IDentifications (PRIDE) database and associated tools: Status in 2013. *Nucleic Acids Res.* *41*, D1063-9.

Wagner, S. A., Satpathy, S., Beli, P. and Choudhary, C. (2016). SPATA2 links CYLD to the TNF-alpha receptor signaling complex and modulates the receptor signaling outcomes. *EMBO J.*

Welch, M. D., DePace, A. H., Verma, S., Iwamatsu, A. and Mitchison, T. J. (1997). The human Arp2/3 complex is composed of evolutionarily conserved subunits and is localized to cellular regions of dynamic actin filament assembly. *J. Cell Biol.* *138*, 375-384.

Wu, C., Asokan, S. B., Berginski, M. E., Haynes, E. M., Sharpless, N. E., Griffith, J. D., Gomez, S. M. and Bear, J. E. (2012). Arp2/3 is critical for lamellipodia and response to extracellular matrix cues but is dispensable for chemotaxis. *Cell* *148*, 973-987.

Wu, J., Vallenius, T., Ovaska, K., Westermarck, J., Makela, T. P. and Hautaniemi, S. (2009). Integrated network analysis platform for protein-protein interactions. *Nat. Methods* *6*, 75-77.

Yang, Y., Kelly, P., Shaffer, A. L., 3rd, Schmitz, R., Yoo, H. M., Liu, X., Huang da, W., Webster, D., Young, R. M., Nakagawa, M. et al. (2016). Targeting non-proteolytic protein ubiquitination for the treatment of diffuse large B cell lymphoma. *Cancer Cell.* *29*, 494-507.

Yang, Y., Schmitz, R., Mitala, J., Whiting, A., Xiao, W., Ceribelli, M., Wright, G. W., Zhao, H., Yang, Y., Xu, W. et al. (2014). Essential role of the linear ubiquitin chain assembly

complex in lymphoma revealed by rare germline polymorphisms. *Cancer. Discov.* *4*, 480-493.

Zak, D. E., Schmitz, F., Gold, E. S., Diercks, A. H., Peschon, J. J., Valvo, J. S., Niemisto, A., Podolsky, I., Fallen, S. G., Suen, R. et al. (2011). Systems analysis identifies an essential role for SHANK-associated RH domain-interacting protein (SHARPIN) in macrophage toll-like receptor 2 (TLR2) responses. *Proc. Natl. Acad. Sci. U. S. A.* *108*, 11536-11541.

Zhang, Y., Huang, H., Zhou, H., Du, T., Zeng, L., Cao, Y., Chen, J., Lai, Y., Li, J., Wang, G. et al. (2014). Activation of nuclear factor kappaB pathway and downstream targets survivin and livin by SHARPIN contributes to the progression and metastasis of prostate cancer. *Cancer* *120*, 3208-3218.

Figures

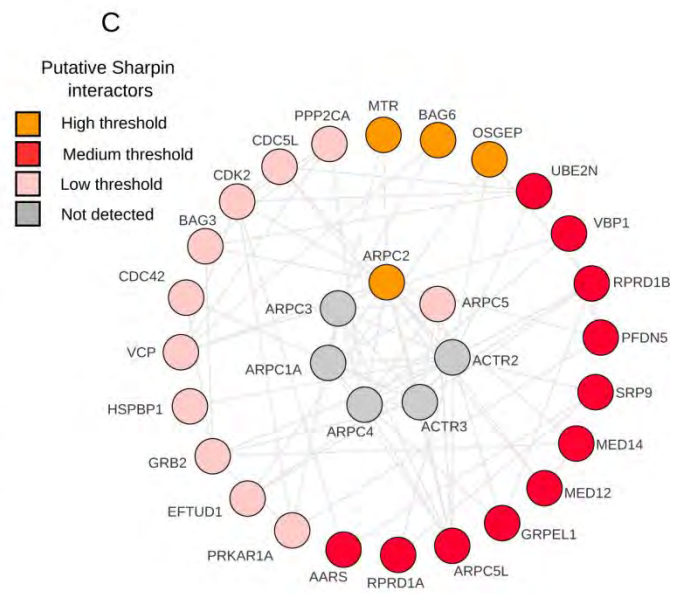
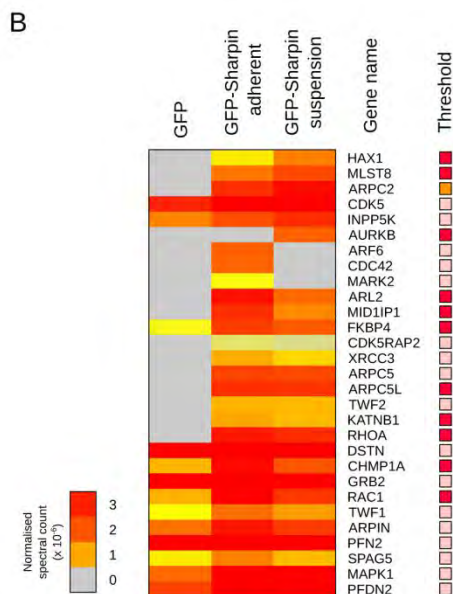
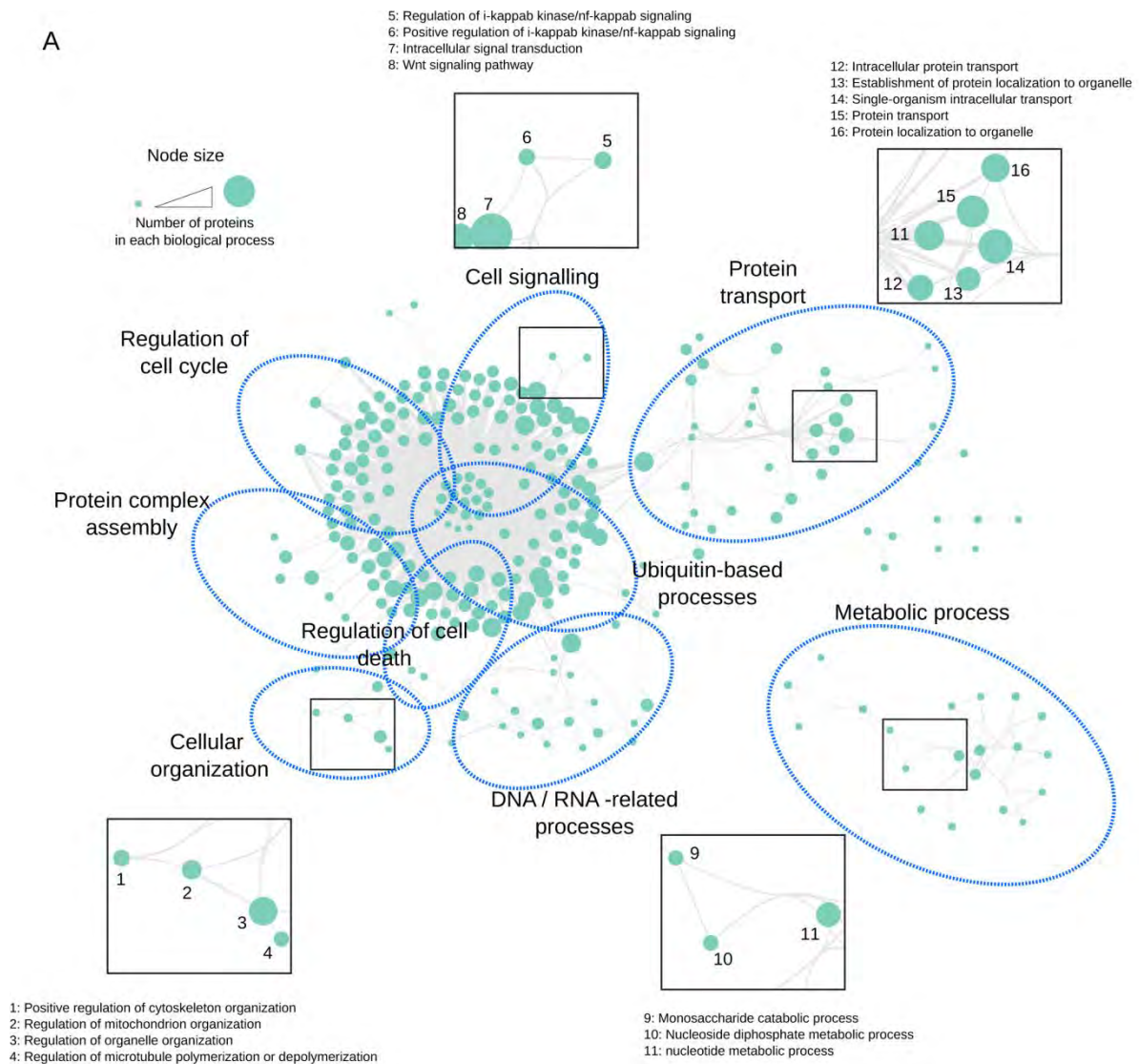


Fig. 1. Gene Ontology and protein network analyses revealed a putative role for Sharpin in regulation of the cytoskeleton. (A) GO-based functional annotation clustering analyses of the proteins recruited to Sharpin. Proteins enriched in the Sharpin pull-downs (medium threshold) were mapped onto the GO category Biological Process (GOTERM_BP_5) using DAVID. 261 GO terms, over-represented in the GFP-Sharpin datasets ($p < 0.05$), were displayed as network-based enrichment maps (see. Table S2 for details). Each node (circle) represents a GO term and each edge (line) connects GO terms that contain at least one common protein. Node area is proportional to the number of proteins that belong to a particular GO term. Nodes of this network were automatically organised using an algorithm that clusters nodes as a function of their connectivity and were then manually annotated. (B) Hierarchical clustering of the putative Sharpin binders (low threshold) annotated with the Gene Ontology term ‘GO:0051493 regulation of cytoskeleton organization’. (C) Proteins identified in the GFP-Sharpin datasets were mapped onto a literature-curated PPI network and a sub-network containing the proteins within one interaction of the Arp2/3 complex was created. Putative Sharpin interactors in (B) and (C) were colour coded to illustrate the threshold of identification.

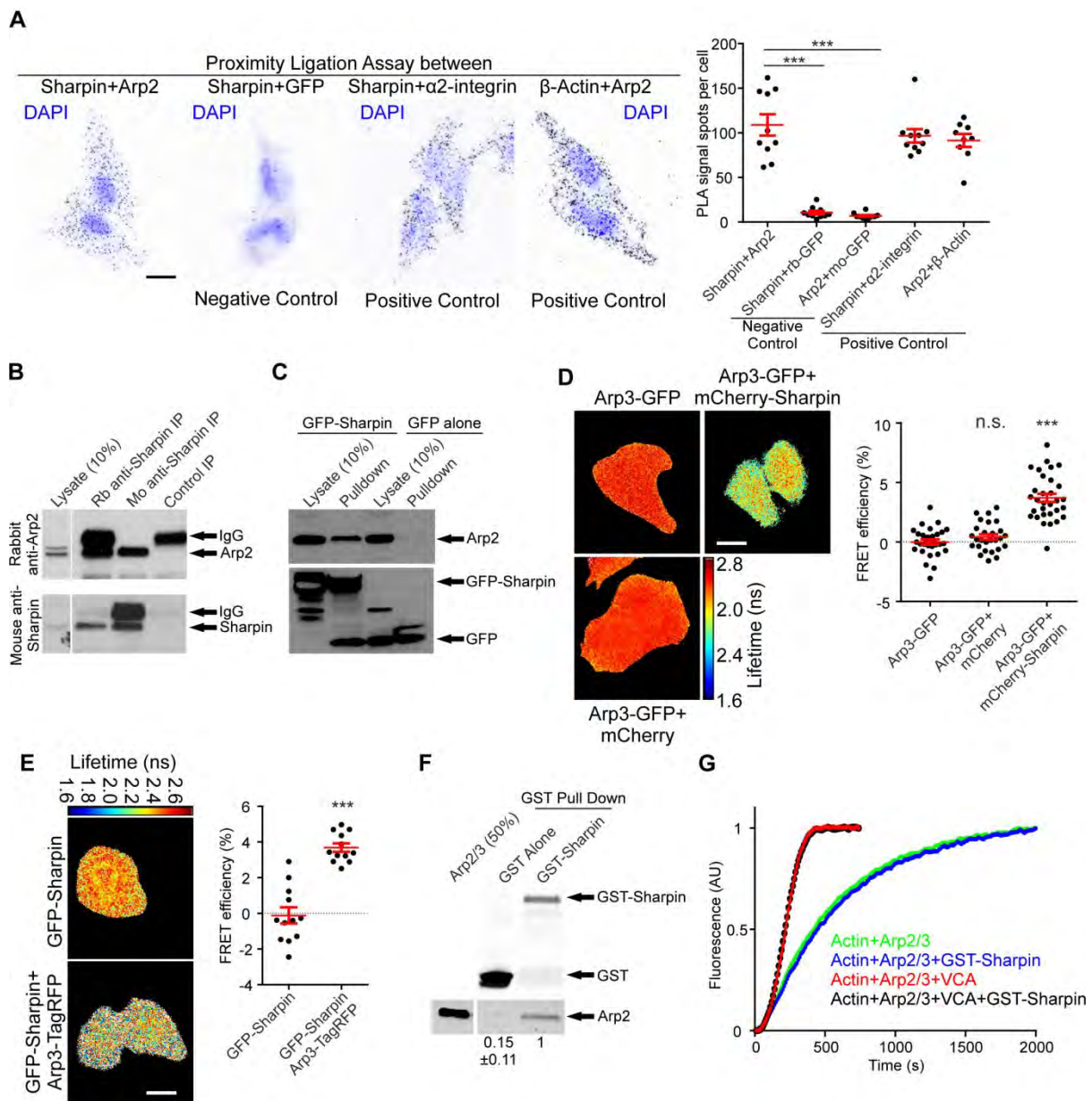


Fig. 2. Sharpin and the Arp2/3 complex interact in cells. (A) PLA with indicated antibody pairs in HeLa cells (rb-GFP and mo-GFP represent mouse and rabbit antibodies against GFP). DAPI indicates nuclei. The graph shows average number of PLA signals (spots) per cell ($n = 10$ images from a representative experiment ($n = 3$ experiments)). (B) Co-immunoprecipitation of endogenous Arp2 and Sharpin using two different Sharpin antibodies (mouse (mo) and rabbit (rb)) from HEK-293 cells (representative from 3 experiments). (C) Pull-down experiments to determine the interaction between GFP or GFP-Sharpin and endogenous Arp2 in HEK-293 cells (representative from 3 experiments). (D,E) HeLa cells

overexpressing the indicated proteins were subjected to FRET analysis by FLIM. Fluorescence lifetimes, mapping spatial FRET in cells, are depicted using a pseudo-colour scale (red-yellow, normal lifetime; yellow-blue, FRET (reduced lifetime)). Graphs show quantification of FRET efficiency (n = (D) 27-31 cells and (E) 12 cells). (F) Pull-down experiment to determine the interaction between recombinant GST or GST-Sharpin and purified bovine Arp2/3 complex. Numerical data are Arp2 levels normalized to GST (n = 3 experiments). (G) Pyrene-actin polymerization assay in the presence of Arp2/3, GST-VCA and GST-Sharpin. Samples of pyrene-actin (4 μ M) were polymerized in the presence of indicated combinations of GST-Sharpin (11 μ M), Arp2/3 (40 nM) and GST-VCA (30 nM) (n = 3 experiments). All numerical data are mean \pm s.e.m. ***: p<0.001. All scale bars are 10 μ m.

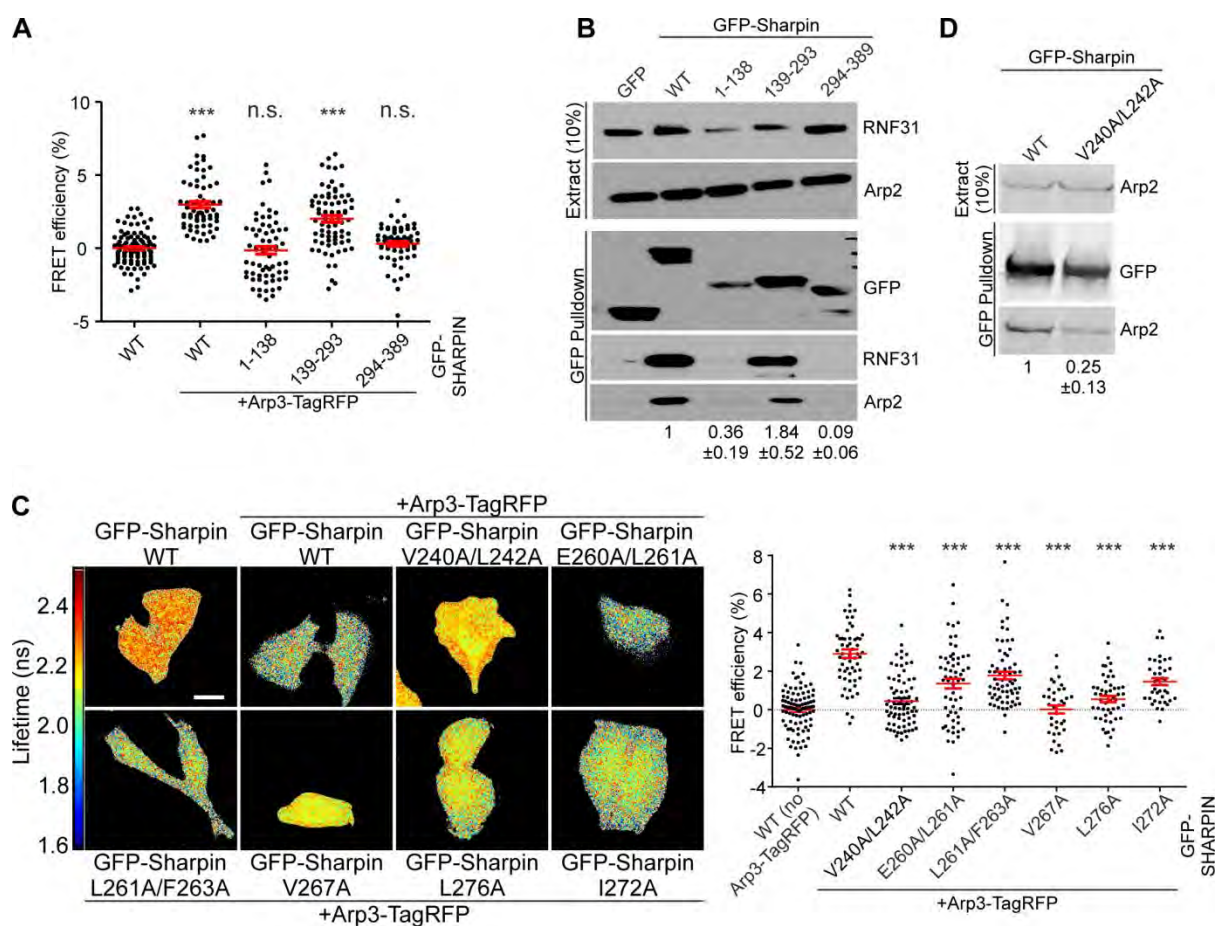


Fig. 3. Mapping the Arp2/3 interaction site of Sharpin. (A) HeLa cells, overexpressing the indicated proteins, were subjected to FRET analysis by FLIM. The graph shows quantification of FRET efficiency ($n = 62-99$ cells, from 3 experiments). (B) Pull-down experiments to determine the interaction between overexpressed GFP-Sharpin WT or fragments and endogenous Arp2 from HEK-293 cells. Blotting for RNF31 confirmed the interaction of RNF31 with the Sharpin UBL domain. Numerical data are Arp2 levels in the pull-down, normalized to Arp2 levels in the extract and GFP levels in the pull-down (3 experiments). (C) HeLa cells, overexpressing the indicated proteins, subjected to FRET analysis by FLIM. Fluorescence lifetimes, mapping spatial FRET in cells, are depicted using a pseudo-colour scale (red-yellow, normal lifetime; yellow-blue, FRET (reduced lifetime)). Scale bar: 10 μm . The graph shows quantification of FRET efficiency ($n = 36-74$ cells, from 3 experiments, donor alone was set to 0 for each individual GFP-Sharpin construct). For

statistical analyses, FRET efficiencies were compared to WT GFP-Sharpin. (D) Pull-down experiments to determine the interaction between overexpressed WT and V240A/L242A GFP-Sharpin and endogenous Arp2 from HEK-293 cells. Numerical data are Arp2 levels in the pulldown, normalized to Arp2 levels in the extract and GFP levels in the pulldown (3 experiments). All numerical data are mean \pm s.e.m. ***: $p < 0.001$.

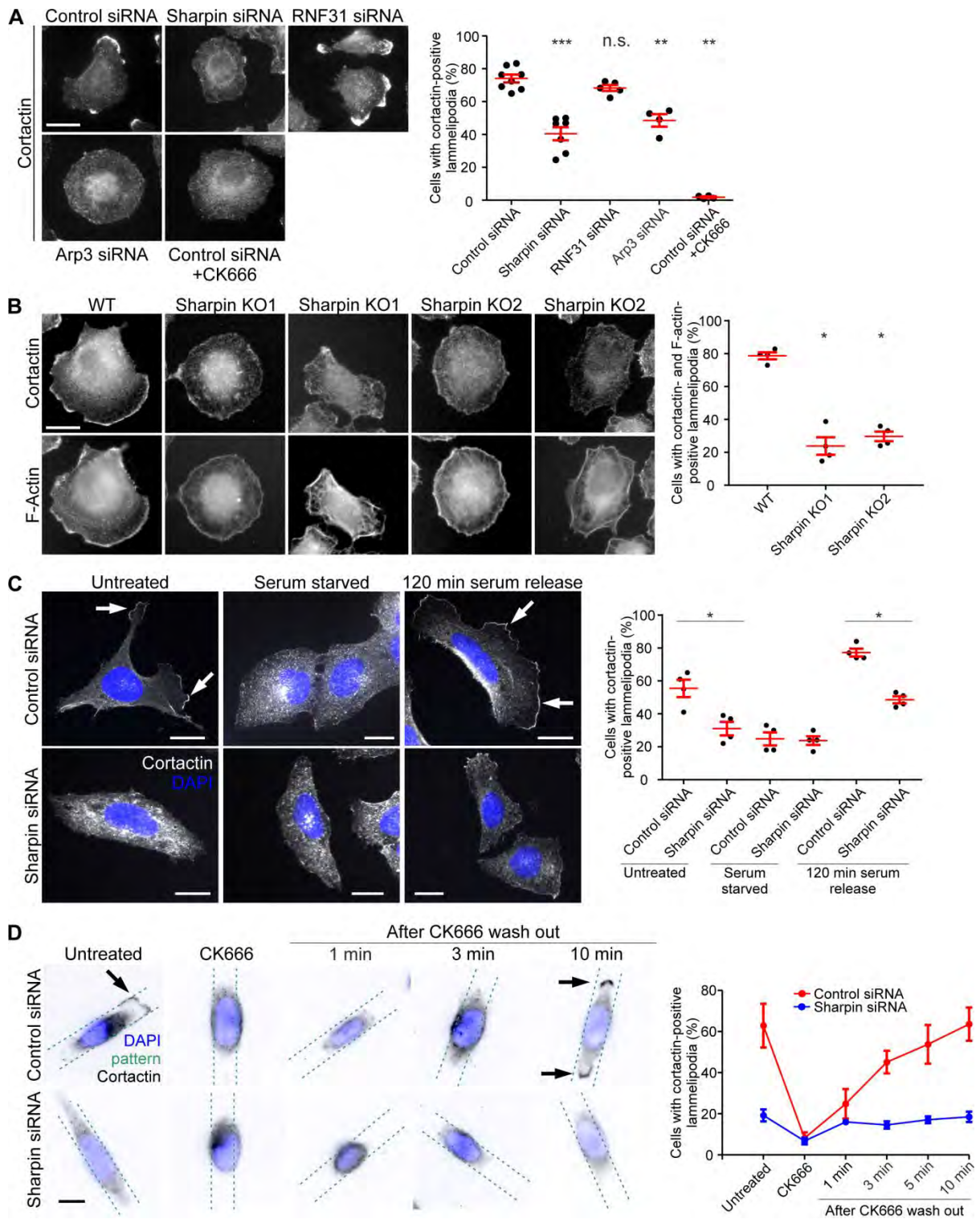


Fig. 4. Sharpin promotes lamellipodium formation. (A) Control, Sharpin, Arp3 and RNF31 silenced NCI-H460 cells, as well as control silenced NCI-H460 cells treated with 100 μ M CK666 for 30 min were stained for cortactin. The graph depicts the percentage of cells with cortactin-positive lamellipodia ($n = 4-9$ experiments, >150 cells per condition per

experiment). (B) WT and two Sharpin knock out NCI-H460 cell lines immunostained for cortactin and F-actin. The graph depicts the percentage of cells with cortactin- and F-actin positive lamellipodia (n = 4 experiments, >125 cells per condition per experiment). (C) Control and Sharpin silenced U2OS cells were grown under normal conditions, serum starved overnight, or released into serum-containing medium for 120 min after overnight serum starvation, and subsequently stained for cortactin. The graph depicts the percentage of cells with cortactin-positive lamellipodia (n = 4 experiments, 20-79 cells per condition per experiment). (D) Control and Sharpin silenced NCI-H460 cells, attached to linear micropatterns, were treated for 30 min with 100 μ M CK666 and then released. Cells were fixed without CK666 treatment, after CK666 treatment and at different time points after release, followed by staining for cortactin (the position of the linear micropatterns is indicated with green dotted lines). The graph shows the percentage of cells with cortactin-positive lamellipodia (n = 3 experiments, 12-40 cells per condition per experiment). All numerical data are mean \pm s.e.m. ***: p<0.001; **: p<0.01; *: p<0.05. All scale bars are 10 μ m. DAPI was used to stain nuclei.

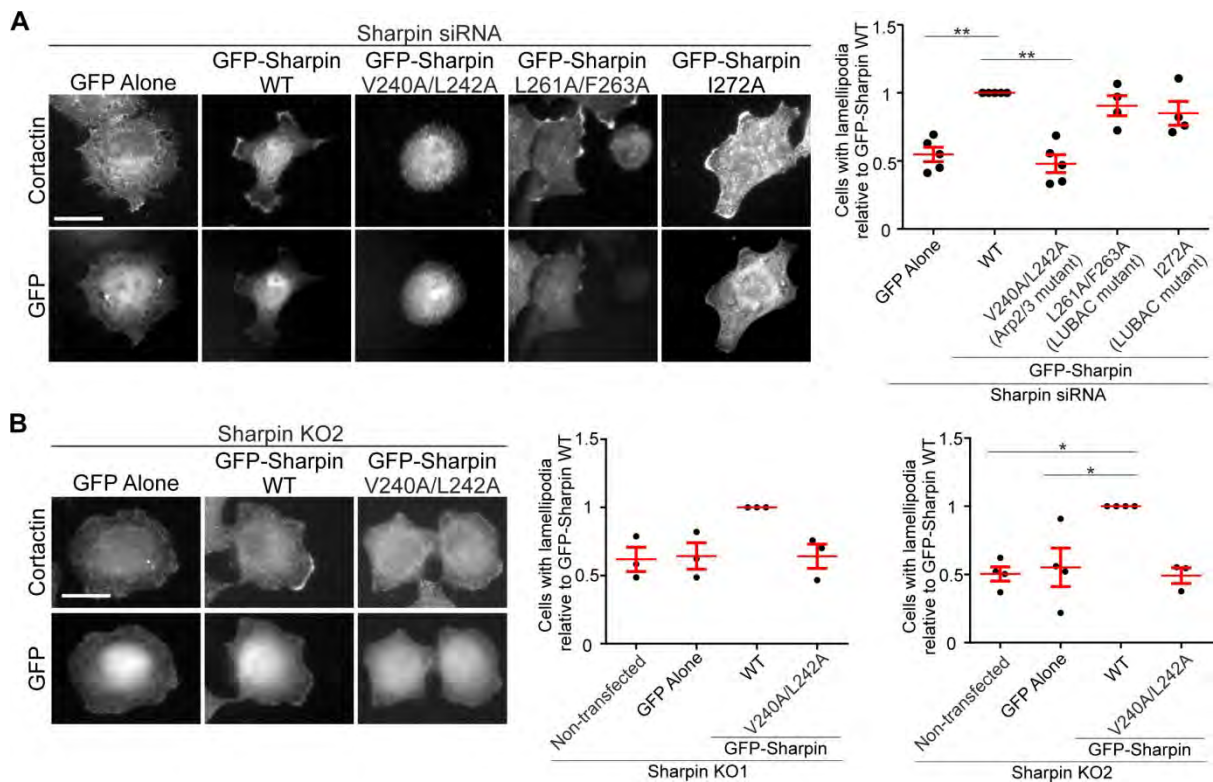


Fig. 5. Sharpin promotes lamellipodium formation through interaction with the Arp2/3 complex. (A) Sharpin silenced NCI-H460 cells or (B) Sharpin KO2 NCI-H460 cells overexpressing the indicated proteins were stained for cortactin. Graphs depict the amount of GFP-positive cells with cortactin-positive lamellipodia, relative to GFP-Sharpin WT, for (A) Sharpin silenced ($n = 4$ experiments, >30 cells per condition per experiment) and (B) Sharpin knock out cells ($n = 3$ or 4 experiments, 19-56 cells per condition per experiment). All numerical data are mean \pm s.e.m. *: $p < 0.05$, **: $p < 0.01$. All scale bars are 10 μm .

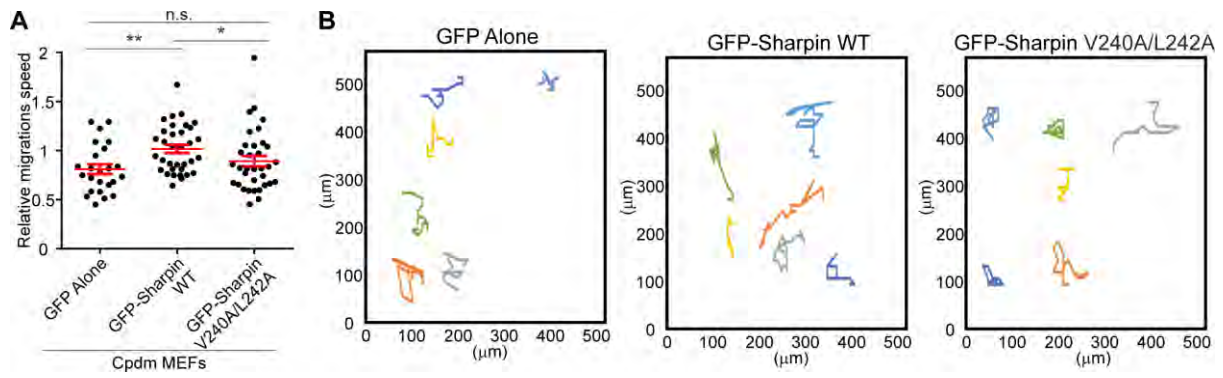
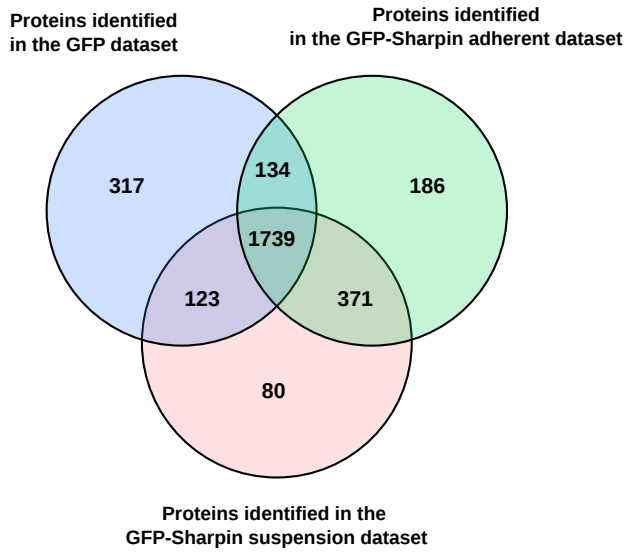


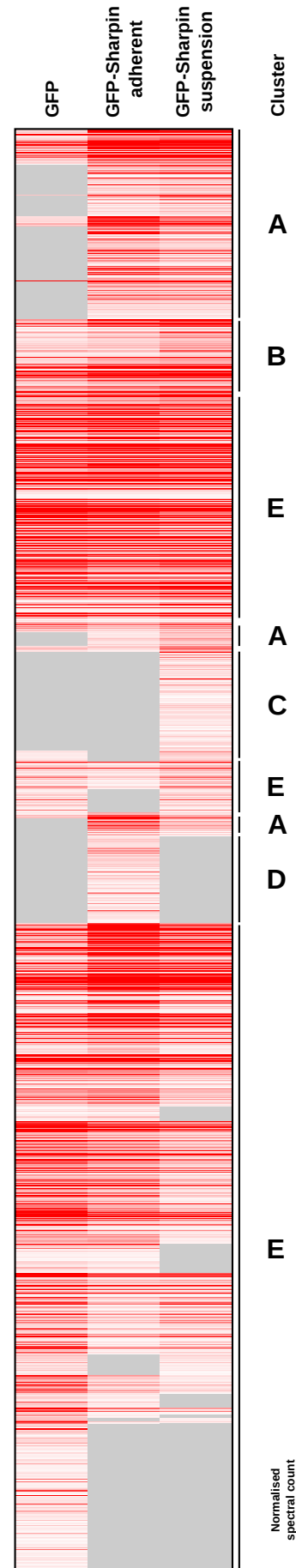
Fig. 6. Sharpin promotes cell migration through interaction with the Arp2/3 complex.

(A) Quantification of migration speed and (B) representative cell tracks (4.5 h) of cpdm MEFs overexpressing GFP alone, WT GFP-Sharpin or V240A/L242A GFP-Sharpin on 5 $\mu\text{g/ml}$ fibronectin (n = 24, 34 and 34 cell respectively, from 3, 4 and 4 experiments (6-10 cells from each experiment)). All numerical data are mean \pm s.e.m. **: $p < 0.01$, *: $p < 0.05$, n.s.: not significant.

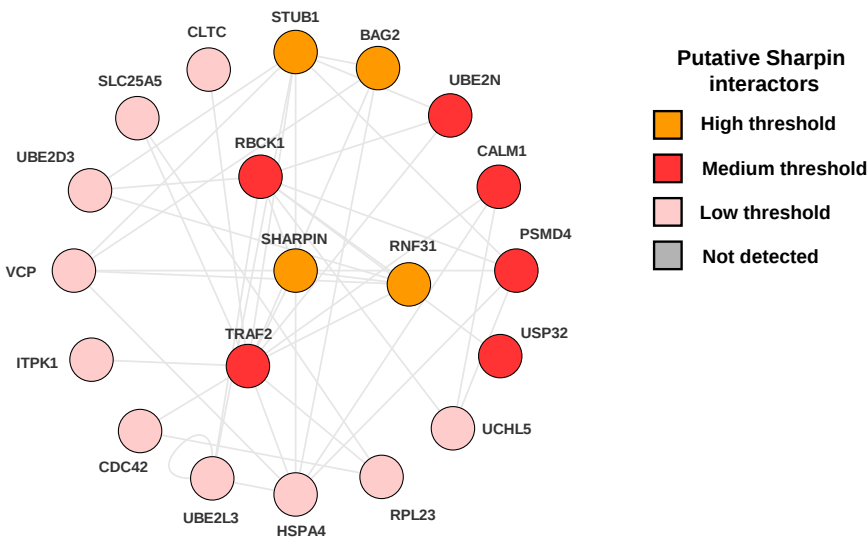
A



B



C



D

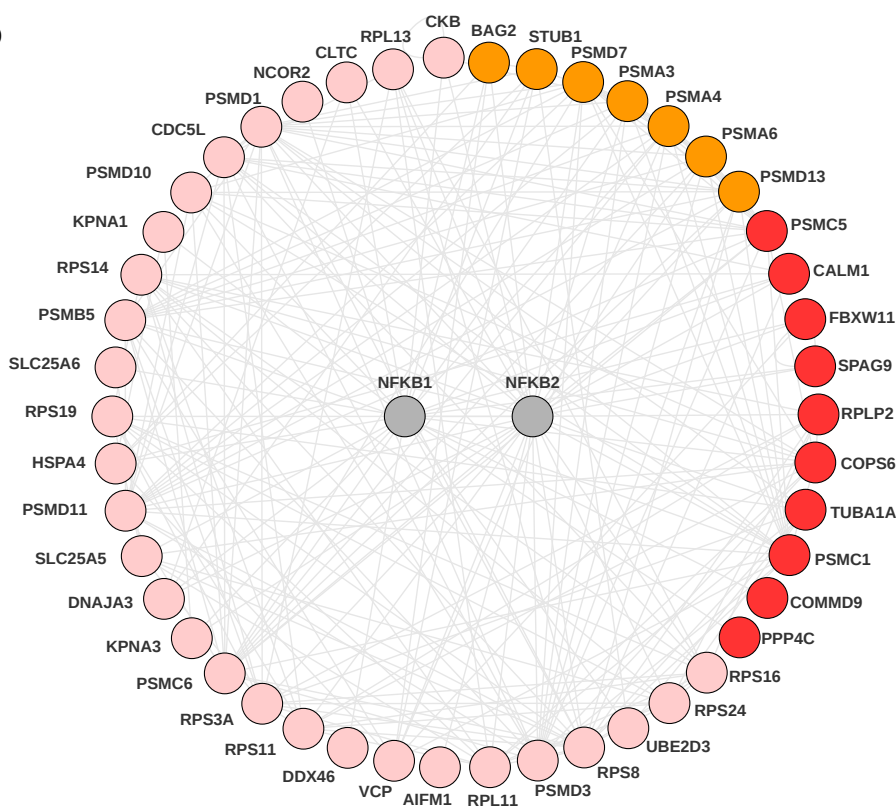
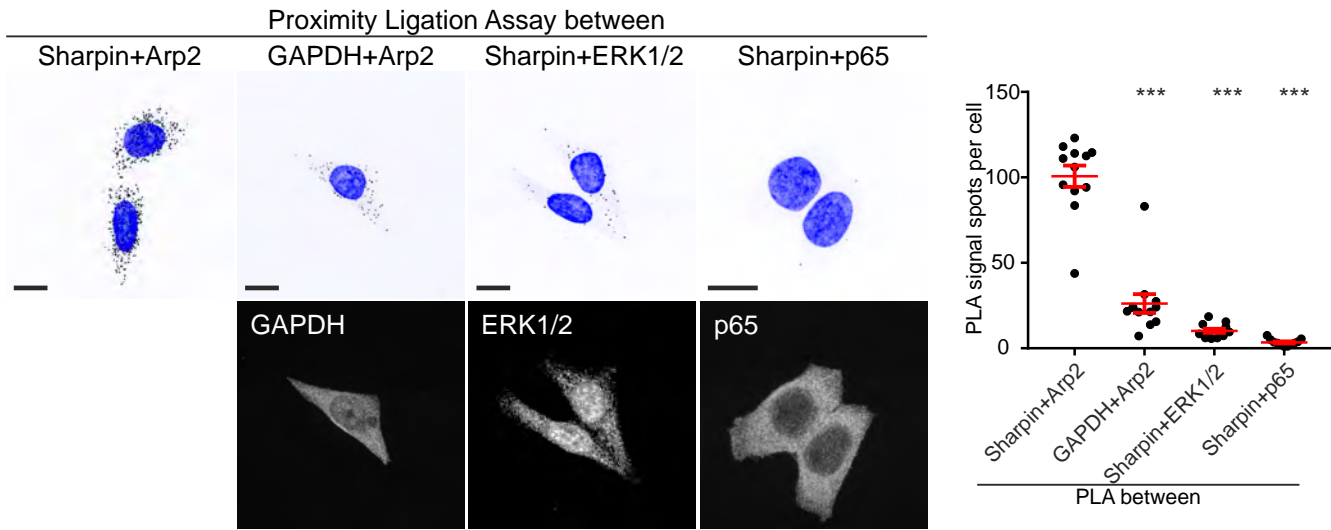
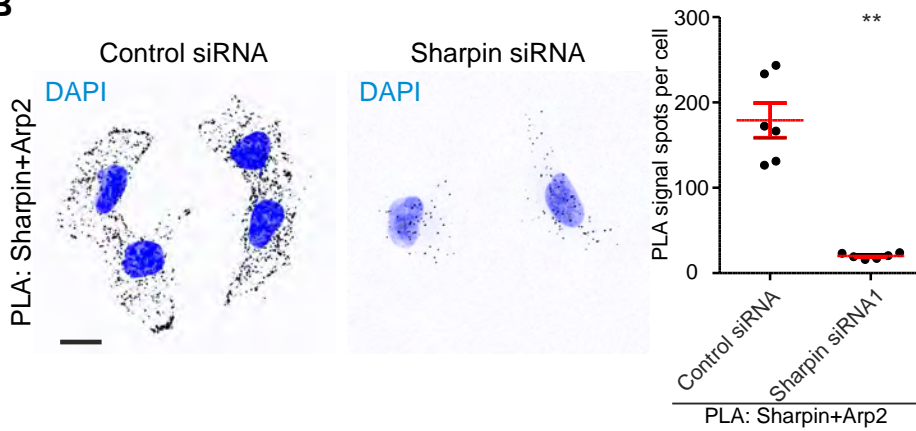


Fig. S1. Proteomic analysis of Sharpin interactors. (A) The distribution of proteins identified in the GFP, GFP-Sharpin suspension and GFP-Sharpin adherent datasets illustrated as a Venn diagram. (B) Hierarchical clustering of proteins identified in the GFP control, GFP-Sharpin suspension and GFP-Sharpin adherent mass spectrometry datasets. Cluster A contains all proteins that were strongly enriched in both GFP-Sharpin adherent and GFP-Sharpin suspension, when compared to GFP alone. Proteins in cluster B are weakly enriched in both GFP-Sharpin adherent and GFP-Sharpin suspension, when compared to GFP alone. Cluster C and D contains those proteins that are specifically enriched in GFP-Sharpin suspension and GFP-Sharpin adherent, respectively. Proteins in cluster E were present in all three experimental conditions or were enriched in GFP alone. (C,D) Proteins identified in the GFP-Sharpin datasets were mapped onto a literature-curated protein-protein interaction network (see methods for details). Sub-networks containing the proteins within two interactions of Sharpin (C) and the proteins within one interaction of NF- κ B were created (D). Each node (circle) represents a protein (labelled with gene name) and each line represents a reported interaction between two proteins. Nodes of this network were colour coded to illustrate the threshold of identification.

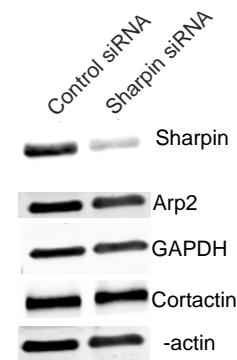
A



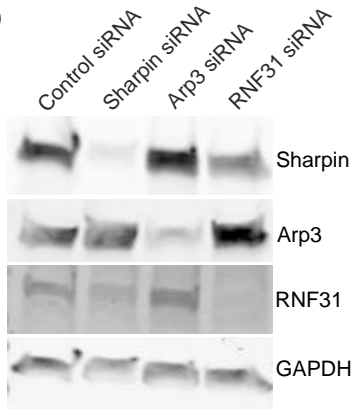
B



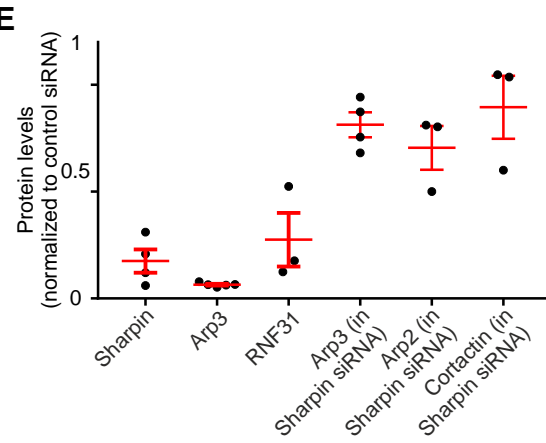
C



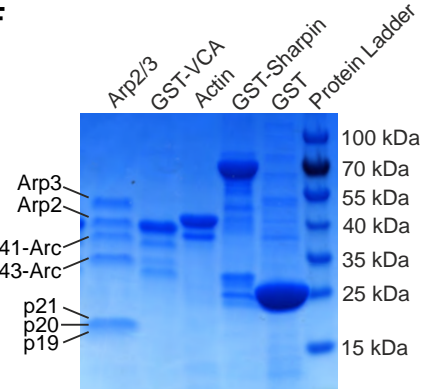
D



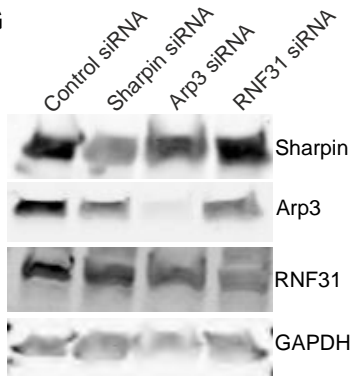
E



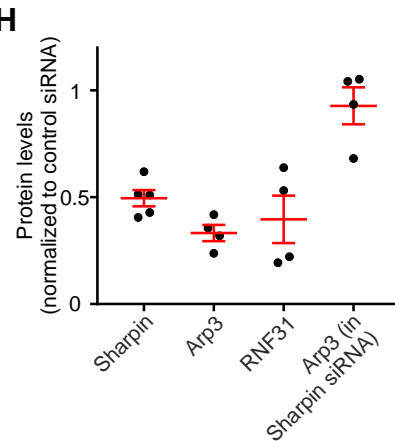
F



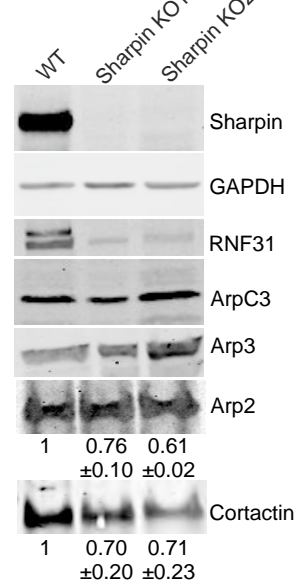
G



H



I



J

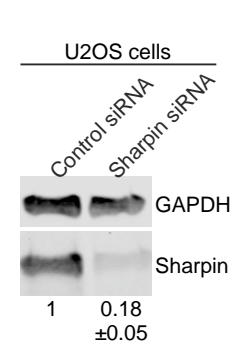


Figure S2. Control proximity ligation, Western blot and Coomassie staining experiments.

(A,B) (A) PLA between Sharpin and Arp2, ERK1/2, or p65 and between Arp2 and GAPDH in untreated HeLa cells and (B) PLA between Sharpin and Arp2 in control and Sharpin silenced HeLa cells. Scale bar: 10 μ m. DAPI was used to stain nuclei. The graphs show average number of PLA signals (spots) per cell ($n = 10$ and 6 images, respectively) from a representative experiment ($n = 3$ experiments). (C,D) Western blot analysis of (C) Sharpin, β -actin, Arp2, cortactin and GAPDH levels in control or Sharpin silenced HeLa cells or (D) Sharpin, Arp3, RNF31 and GAPDH levels in Control, Sharpin, Arp3 or RNF31 silenced HeLa cells. (E) From blots as show in (C,D) residual Sharpin, Arp3 and RNF31 levels in cells transfected with their respective siRNAs ($n = 3-5$), as well as Arp2, Arp3 and Cortactin levels in Sharpin silenced cells ($n = 3$ or 4) were quantified (normalized to GAPDH and control silenced cells). (F) Coomassie staining to show the purity and concentration of the purified and recombinant proteins used. Similar amounts of protein were loaded per lane (4 μ g of Arp2/3, GST-VCA and Actin, 7.1 μ g GST-Sharpin and 15.3 μ g GST only). (G) Sharpin, Arp3, RNF31 and GAPDH levels in Control, Sharpin, Arp3 or RNF31 silenced NCI-H460 cells. (H) From blots as show in (G) residual Sharpin, Arp3 and RNF31 levels in cells transfected with their respective siRNAs ($n = 4$ or 5), as well as Arp3 levels in Sharpin silenced cells ($n = 4$) were quantified (normalized to GAPDH and control silenced cells). (I) Sharpin, GAPDH, RNF31, Arp2, Arp3, cortactin and ArpC3 levels in WT and Sharpin knock out cell lines created using CRISPR. Numerical data are Arp2 and Cortactin levels, normalized to GAPDH levels ($n = 6$). (J) Sharpin and GAPDH levels in Control and Sharpin silenced U2OS cells. Numerical data are Sharpin levels, normalized to GAPDH levels ($n = 3$). All numerical data are mean \pm s.e.m. ***: $p < 0.001$, **: $p < 0.01$.

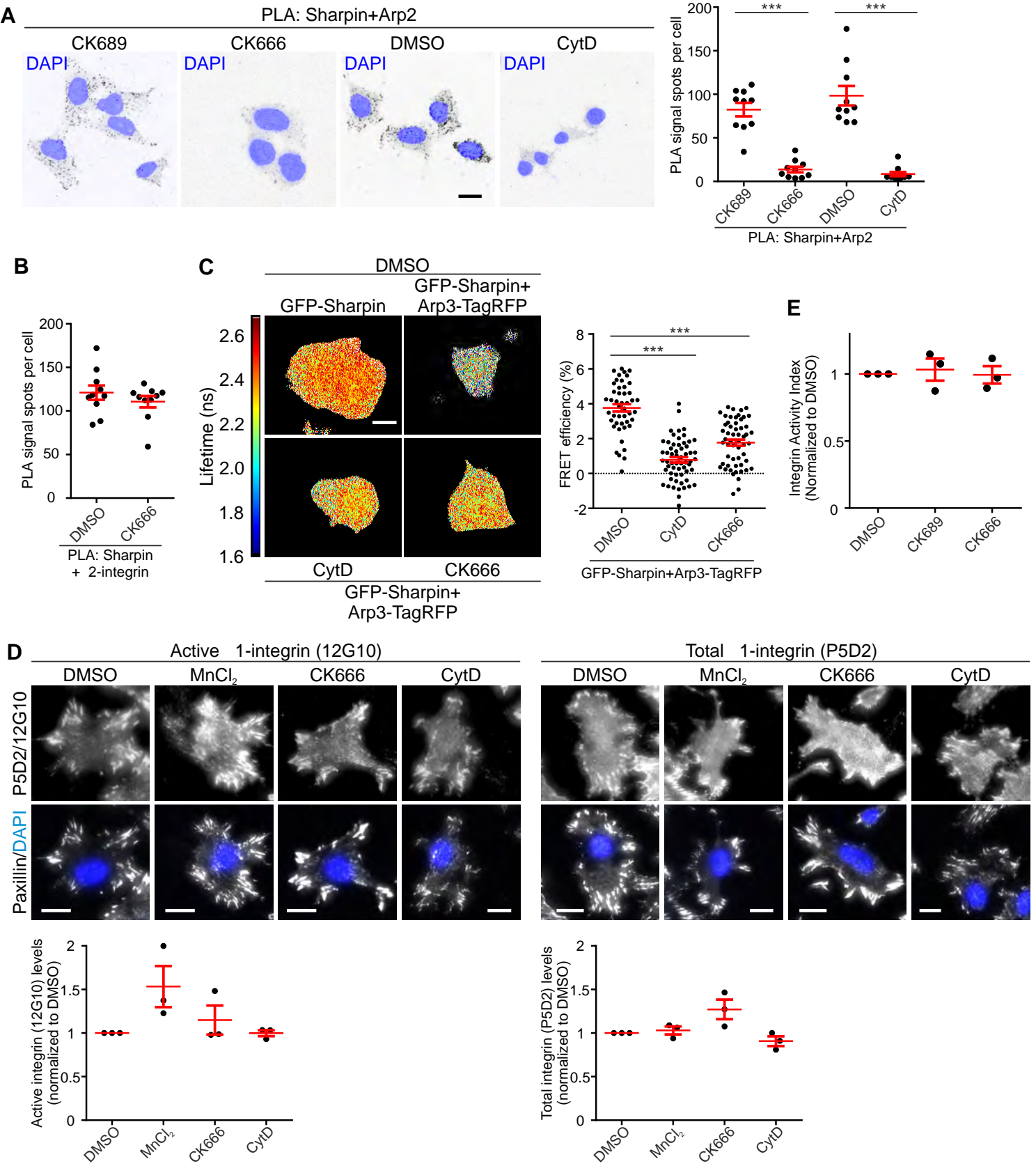


Figure S3. The Sharpin-Arp2/3 interaction depends on an intact cytoskeleton and Arp2/3 activity. (A) PLA between Sharpin and Arp2 in HeLa cells treated for 30 min with DMSO, 10 μ M Cytochalasin D (CytD), 100 μ M CK689 (an inactive analogue of CK666) or 100 μ M CK666. Scale bar: 10 μ m, DAPI was used to stain nuclei. The graph shows the average number of PLA signals (spots) per cell ($n = 10$ images) from a representative experiment ($n = 3$ experiments). (B) Quantification of PLA between Sharpin and $\alpha 2$ -integrin in HeLa cells treated for 30 min with DMSO or 100 μ M CK666. The graph shows average number of PLA signals per cell ($n = 10$ images) from a representative experiment ($n = 2$ experiments). (C) HeLa cells, overexpressing GFP-Sharpin WT alone or GFP-Sharpin in combination with Arp3-TagRFP and treated for 30 min with DMSO, 10 μ M Cytochalasin D (CytD) or 100 μ M CK666 as indicated, were subjected to FRET analysis by FLIM. Fluorescence lifetimes, mapping spatial FRET in cells, are depicted using a pseudo-colour scale (red-yellow, normal lifetime; yellow-blue, FRET (reduced lifetime)). Scale bar: 10 μ m. The graph shows quantification of FRET efficiency ($n = 46$ -59 cells from 3 individual experiments). (D) HeLa cells, freshly adherent to 5 μ g/ml fibronectin, were treated 2h with DMSO, 2h with 2 μ M $MnCl_2$, 1h with 100 μ M CK666 or 15 min with 10 μ M CytD, so that the total adhesion time was 4h for all conditions. Cells were stained for paxillin (a marker for integrin adhesions), nuclei (DAPI) and active $\beta 1$ -integrin (12G10; left panel) or total $\beta 1$ -integrin (P5D2; right panel), and imaged using TIRF microscopy. The graphs show average 12G10 and P5D2 levels per cell, normalized to DMSO control ($n = 3$ experiments; 15-45 cells were analysed per condition per experiment). Treatment with $MnCl_2$ was used as a positive control for integrin activation. (E) FACS analysis of HeLa cells treated for 30 min with DMSO, 100 μ M CK689 or 100 μ M CK666 and stained using antibodies recognizing active $\beta 1$ -integrin (12G10) and total $\beta 1$ -integrin (P5D2). The Integrin Activation Index was calculated by dividing active cell-surface integrin levels (12G10 binding minus secondary only) by total cell-surface integrin levels (P5D2 staining minus secondary antibody alone) ($n = 3$). All numerical data are mean \pm s.e.m. ***: $p < 0.001$.

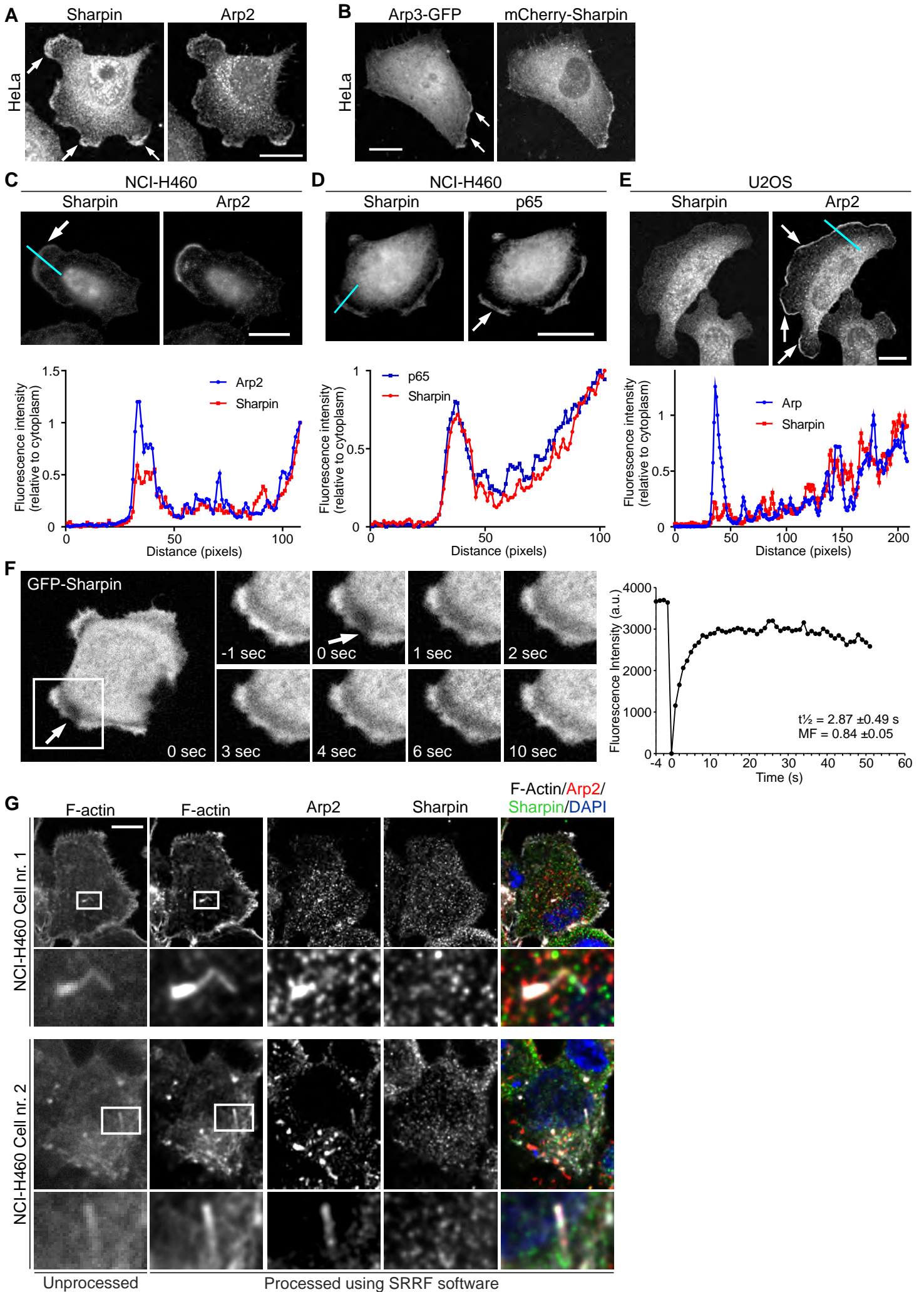


Figure S4. Localization of Sharpin and the Arp2/3 complex in cells. (A,B) Localization of (A) endogenous Sharpin and Arp2 or (B) mCherry-Sharpin and Arp3-GFP in HeLa cells. Arrows indicate lamellipodia. (C-E) NCI-H460 cells immunostained for (C) Sharpin and Arp2 or (D) Sharpin and p65, and (E) U2OS cells immunostained for Sharpin and Arp2. Arrows indicate lamellipodia. Graphs show representative line scans, which plot Sharpin and Arp2 or p65 intensities (background corrected and normalized to cytoplasmic levels) along a line from outside the cell, across a lamellipodium, into the cytoplasm (such as indicated by the blue lines). (F) Time-lapse images of a GFP-Sharpin expressing NCI-H460 cell. GFP fluorescence was bleached in part of the lamellipodium, indicated by the arrow, just before $t = 0$ sec. The graph displays FRAP kinetics from a representative cell. The halftime of recovery ($t_{1/2}$) and mobile fraction are shown as mean \pm s.e.m. ($n = 19$ lamellipodia from 2 experiments). (G) Two individual Myc-PIP5KIb-expressing NCI-H460 cells stained for Sharpin, Arp2, F-actin and nucleus (DAPI). Left panel shows an unprocessed F-actin staining while the other panels show images that were processed using the SRRF ImageJ plugin. Lower panels show enlarged areas with a PIP5KIb-induced actin comet. All scale bars: 10 μ m.

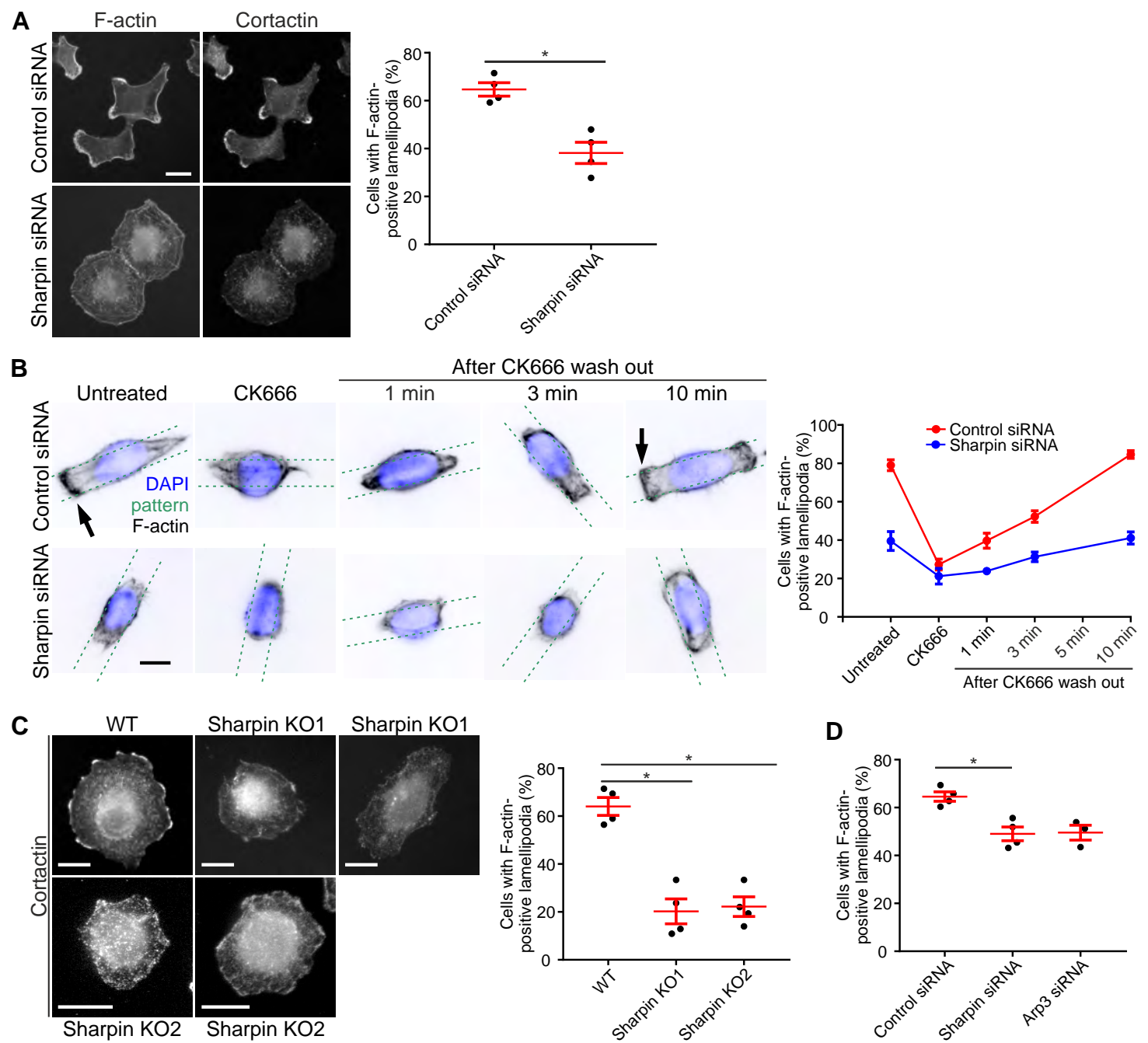


Figure S5. Sharpin promotes lamellipodium formation. (A) Control and Sharpin silenced NCI-H460 cells were stained for F-actin and cortactin. The graph depicts the percentage of cells with F-actin-positive lamellipodia (n = 4 individual experiments, >40 cells per condition in each experiment). (B) Control and Sharpin silenced NCI-H460 cells, attached to linear micropatterns (50 μ g/ml fibronectin and 5 μ g/ml Alexa Fluor488 Conjugated Fibrinogen from

Human plasma), were treated for 30 min with 100 μ M CK666 and then released. Cells were fixed without CK666 treatment, after the CK666 treatment and at different time points after release, followed by staining for F-actin and nuclei (DAPI). The position of the linear micropatterns is indicated with green dotted lines. The graph shows quantification of the percentage of cells with F-actin-positive lamellipodia ($n = 3$ individual experiments, 16-77 cells per condition per experiment). (C) WT and Sharpin knock out NCI-H460 cells, spreading for 3h on 5 μ g/ml fibronectin, were stained for cortactin. The graphs depicts the percentage of cells with cortactin-positive lamellipodia ($n = 4$ individual experiments, >49 cells per condition in each experiment). (D) Graph depicting the percentage of control, Sharpin and Arp3 silenced NCI-H460 cells, spreading for 3h on 5 μ g/ml fibronectin, with cortactin-positive lamellipodia ($n = 4$ (control and Sharpin siRNA) or 3 (Arp3 siRNA) individual experiments, >40 cells per condition in each experiment). All numerical data are mean \pm s.e.m. *: $p < 0.05$. All scale bars are 10 μ m.

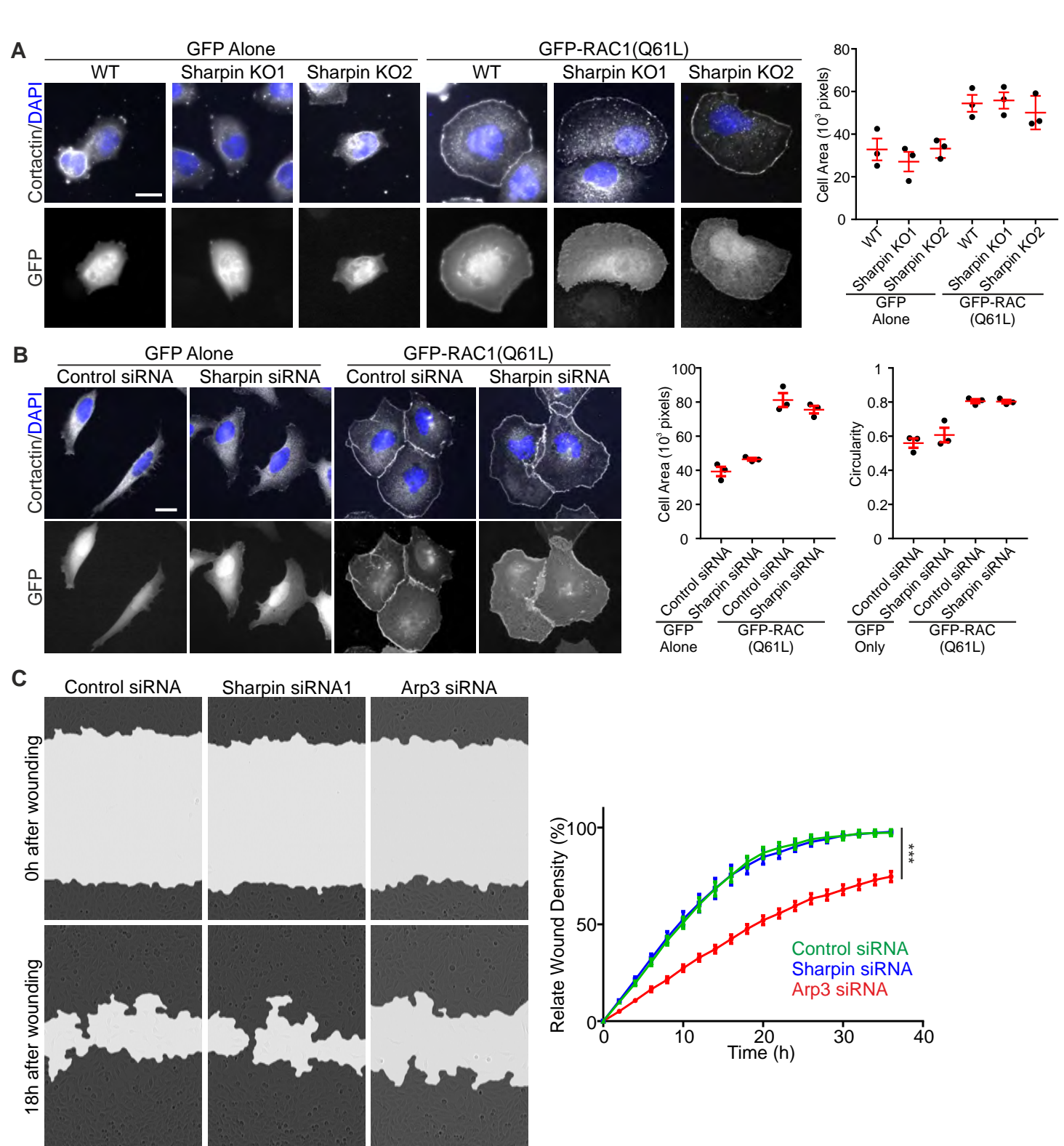


Figure S6. (A,B) WT, Sharpin KO1 and Sharpin KO2 NCI-H460 cells (A) or Control and Sharpin silenced HeLa cells (B) expressing constitutively active GFP-RAC1(Q61L) or GFP alone were stained for cortactin and nuclei (DAPI). Graph shows quantification of (A,B) cell area and (B) circularity (n = 3 individual experiments, 20-40 (A) or 15-30 (B) cells per

condition in each experiment). Numerical data are mean \pm s.e.m. Scale bar is 10 μ m. (C) Control, Sharnin or Arp3 silenced HeLa cells were grown to confluency in 96 well plate wells. The wound was imaged every 2 h for 72 h. Micrographs depict the wound at 0h and 22h after wounding (a grey mask marks the wound). The graph shows percentage of wound closure over time (n = 3 experiments with 4-6 wells per condition). All numerical data are mean \pm s.e.m. ***: p<0.001.

Table S1

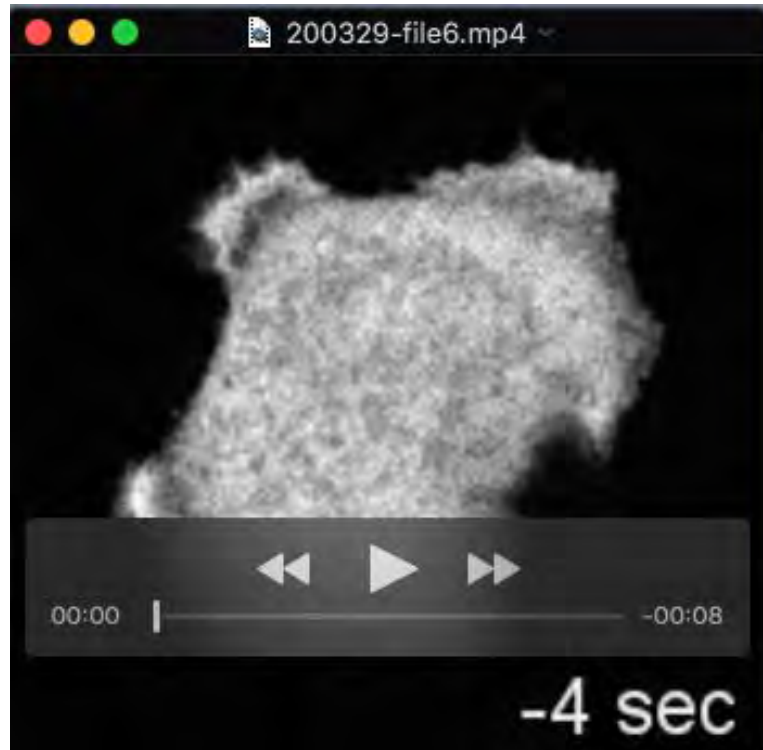
[Click here to Download Table S1](#)

Table S2

[Click here to Download Table S2](#)

Table S3

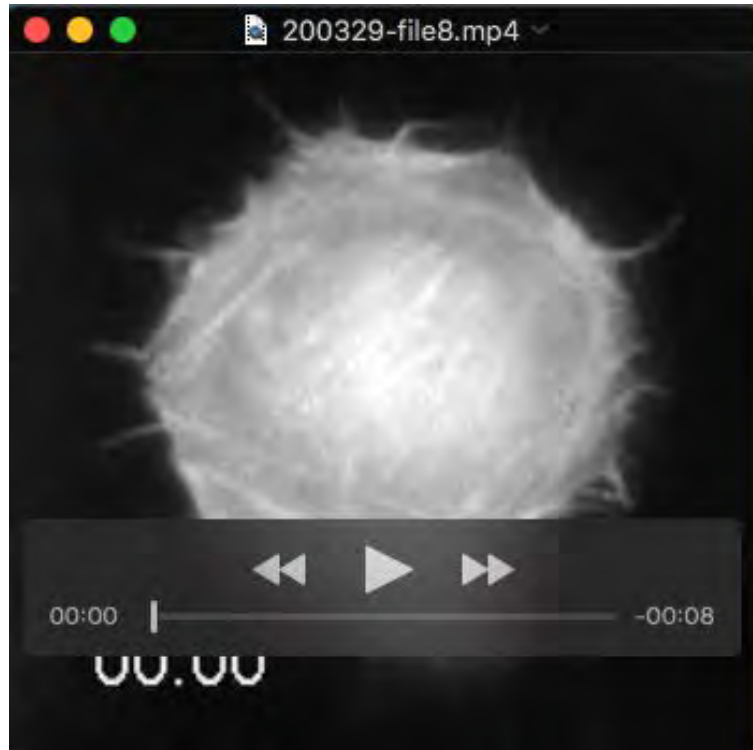
[Click here to Download Table S3](#)



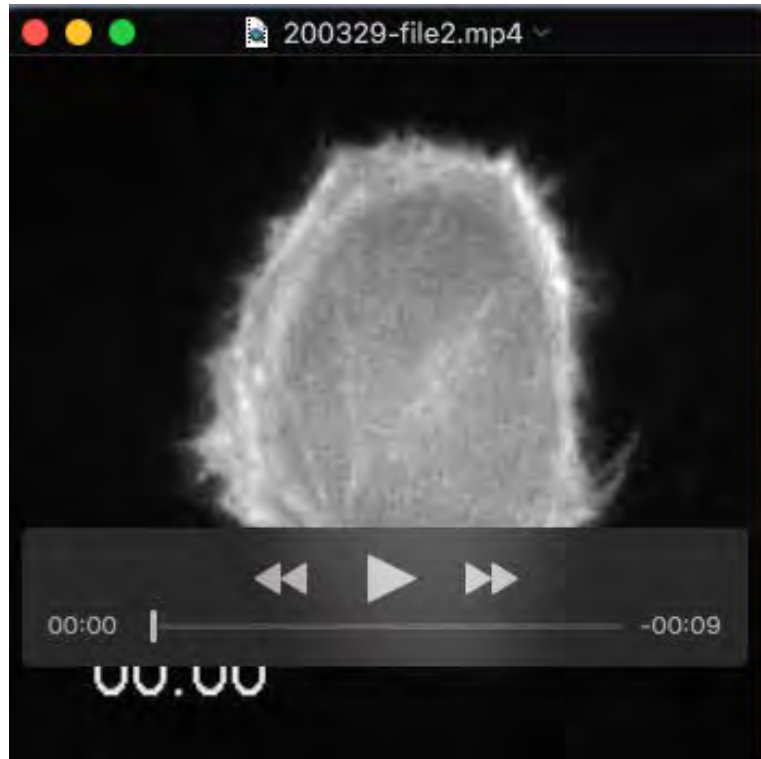
Movie S1. Time-lapse imaging of a GFP-Sharpin overexpressing NCI-H460 cell. GFP fluorescence was bleached in part of the lamellipodium just before $t = 0$ sec.



Movie S2. Time-lapse imaging of a control silenced NCI-H460 cell expressing mEmerald-Lifact.



Movie S3. Time-lapse imaging of a Sharpin silenced NCI-H460 cell expressing mEmerald-Lifeact.



Movie S4. Time-lapse imaging of an Arp3 silenced NCI-H460 cell expressing mEmerald-Lifeact.